UNLV | UNIVERSITY LIBRARIES

UNLV Retrospective Theses & Dissertations

1-1-2000

The contribution of construction materials to the airborne radon concentrations in an underground facility

Robert Arthur Brounstein
University of Nevada, Las Vegas

Follow this and additional works at: https://digitalscholarship.unlv.edu/rtds

Repository Citation

Brounstein, Robert Arthur, "The contribution of construction materials to the airborne radon concentrations in an underground facility" (2000). *UNLV Retrospective Theses & Dissertations*. 1231.
http://dx.doi.org/10.25669/qred-9pea

This Thesis is protected by copyright and/or related rights. It has been brought to you by Digital Scholarship@UNLV with permission from the rights-holder(s). You are free to use this Thesis in any way that is permitted by the copyright and related rights legislation that applies to your use. For other uses you need to obtain permission from the rights-holder(s) directly, unless additional rights are indicated by a Creative Commons license in the record and/or on the work itself.

This Thesis has been accepted for inclusion in UNLV Retrospective Theses & Dissertations by an authorized administrator of Digital Scholarship@UNLV. For more information, please contact digitalscholarship@unlv.edu.

INFORMATION TO USERS

This manuscript has been reproduced from the microfilm master. UMI films the text directly from the original or copy submitted. Thus, some thesis and dissertation copies are in typewriter face, while others may be from any type of computer printer.

The quality of this reproduction is dependent upon the quality of the copy submitted. Broken or indistinct print, colored or poor quality illustrations and photographs, print bleedthrough, substandard margins, and improper alignment can adversely affect reproduction.

In the unlikely event that the author did not send UMI a complete manuscript and there are missing pages, these will be noted. Also, if unauthorized copyright material had to be removed, a note will indicate the deletion.

Oversize materials (e.g., maps, drawings, charts) are reproduced by sectioning the original, beginning at the upper left-hand corner and continuing from left to right in equal sections with small overlaps.

Photographs included in the original manuscript have been reproduced xerographically in this copy. Higher quality 6" x 9" black and white photographic prints are available for any photographs or illustrations appearing in this copy for an additional charge. Contact UMI directly to order.

Bell & Howell Information and Learning
300 North Zeeb Road, Ann Arbor, MI 48106-1346 USA
800-521-0600

UMI®

Reproduced with permission of the copyright owner. Further reproduction prohibited without permission.

Reproduced with permission of the copyright owner. Further reproduction prohibited without permission.

THE CONTRIBUTION OF CONSTRUCTION MATERIALS TO THE AIRBORNE RADON CONCENTRATIONS IN AN UNDERGROUND FACILITY

by

Robert A. Brounstein

Bachelor of Science, Chemical Engineering
California Polytechnic University, Pomona, California
1986

A thesis submitted in partial fulfillment
of the requirements for the degree of

Master of Science Degree
Department of Health Physics
College of Health Sciences

Graduate College
University of Nevada, Las Vegas
December 2000

Reproduced with permission of the copyright owner. Further reproduction prohibited without permission.

UMI Number: 1403246

UMI®

UMI Microform 1403246
Copyright 2001 by Bell & Howell Information and Learning Company.
All rights reserved. This microform edition is protected against
unauthorized copying under Title 17, United States Code.

Bell & Howell Information and Learning Company
300 North Zeeb Road
P.O. Box 1346
Ann Arbor, MI 48106-1346

Reproduced with permission of the copyright owner. Further reproduction prohibited without permission.

UNLV
UNLV

Thesis Approval
The Graduate College
University of Nevada, Las Vegas

October 20, 2000, 20___

The Thesis prepared by

Robert A. Brounstein

Entitled

The Contribution of Construction Materials to the Airborne Radon Concentrations in an Underground Facility

is approved in partial fulfillment of the requirements for the degree of

Master of Science

Examination Committee Chair

Dean of the Graduate College

Examination Committee Member

Examination Committee Member

Graduate College Faculty Representative

PR/1017-53/1-00

Reproduced with permission of the copyright owner. Further reproduction prohibited without permission.

ABSTRACT

The Contribution of Construction Materials to the Airborne Radon Concentrations in an Underground Facility

by

Robert A. Brounstein

Dr. Mark J. Rudin, Examination Committee Chair
Professor of Health Physics
University of Nevada, Las Vegas

The radon concentrations within fiber crete and the native material from the U1a Complex at the Nevada Tests Site, Nye County, Nevada, were quantified and compared to each other. Gamma spectroscopy measurements resulted in an average ^{222}Rn concentration to be 0.038 ± 0.0011 and 0.014 ± 0.001 Bq g^{-1} for the native material and fiber crete, respectively. The emanation of ^{222}Rn from the host material was measured via lucas cell scintillation. The average emanation coefficients were significantly higher for the cured fiber crete at 0.07 than for the native material at 0.005. While the cured fiber crete emanation coefficients matched the expected literature values, the coefficient for the native material measured much lower than its expected literature value. Exhalation rates, the amount of radon gas that actually diffuses from the soil gas to the ambient air, were sampled with passive diffusion charcoal canisters. Results, measured by gamma spectroscopy, indicate the average exhalation rate for the native material

Reproduced with permission of the copyright owner. Further reproduction prohibited without permission.

surfaces was 0.0021 ± 0.0002 Bq cm^{-2} hr^{-1}; much higher than that for the fiber crete surface at 0.00099 ± 0.00025 Bq cm^{-2} hr^{-1}.

Reproduced with permission of the copyright owner. Further reproduction prohibited without permission.

TABLE OF CONTENTS

ABSTRACT iii

ACKNOWLEDGEMENTS x

CHAPTER I INTRODUCTION 1
1.1 Occupational and Non-Occupational Radon Exposures 1
1.2 Properties of Radon 3
1.3 Emanation Coefficients 6
1.4 Exhalation 13
1.5 Radon and Radon Progeny 16
1.6 Natural Radioactivity in Materials 19
1.7 Hypothesis 22

CHAPTER II METHODS AND MATERIALS 24
2.1 The U1a Complex 24
2.2 Regional and Site Geology 26
2.3 Mining Application 30
2.4 Fiber Crete 33
2.5 Sampling and Analytical Strategy 34
2.5.1 Initial Collection of Soils and Fiber Crete and Analysis by (-Spectroscopy 34
2.5.2 Collection of Soils and Fiber Crete with Analysis by Scintillation.. 36
2.6 Radon Exhalation Analysis with Charcoal Canisters 42
2.6.1 Measurement of Diffusion Barrier Charcoal Canisters 42
2.6.2 In-Situ Sampling 45

CHAPTER III RESULTS 48
3.1 Analysis of Native Materials and Fiber Crete 48
3.2 Lucas Cell Analysis 64
3.3 Exhalation – Charcoal Canisters 70

CHAPTER IV DISCUSSION 88
4.1 Analysis of Native Materials and Fiber Crete 88
4.2 Lucas Cell Analysis Via Scintillation Measurement 92
4.3 Exhalation Measurements from Charcoal Canisters 98

Reproduced with permission of the copyright owner. Further reproduction prohibited without permission.

CHAPTER V CONCLUSION 108
5.1 Gamma Spectroscopy 108
5.2 Radon Emanation 108
5.3 In-Situ Sampling via Passive Diffusion Charcoal Canisters 109

CHAPTER VI FUTURE WORK 110

REFERENCES 112

VITA 116

Reproduced with permission of the copyright owner. Further reproduction prohibited without permission.

LIST OF FIGURES

Figure 2.1 The U1a Complex 25
Figure 2.2 500-ml HDPE Bottle Connected to Lucas Cell 40
Figure 2.3 Lucas Cell Placed on Photomultiplier Tube with Scalar 41
Figure 3.1 A Comparison of Native Materials and Fiber Crete 80
Figure 3.2 First Round In-Situ Sampling with Unsealed Canisters 84
Figure 3.3 Second Round In-Situ Sampling with Sealed Canisters 85
Figure 3.4 A Comparison of Native Materials and Fiber Crete 87
Figure 4.1 Activities for ^{214}Pb, ^{214}Bi and ^{234}Th for Native Materials 90
Figure 4.2 Emanation Coefficients 93
Figure 4.3 Environmental Conditions During First Round Sampling 102

Reproduced with permission of the copyright owner. Further reproduction prohibited without permission.

LIST OF TABLES

Table 1.1 Measurements of ^{222}Rn Emanation Coefficients 7
Table 1.2 Emanation Coefficients of Some Building Materials 10
Table 1.3 Radon Exhalation Rates of Some Building Materials 14
Table 1.4 ^{226}Ra Concentrations in Various Types of Rocks 20
Table 2.1 Comparison of Physical Property Results in U1a 29
Table 3.1 Physical Data for Gamma Spectropscopy, Native Material (First round Sampling) 49
Table 3.2 Physical Data for Gamma Spectropscopy, Native Material of In-Situ Location 49
Table 3.3 Physical Data for Gamma Spectropscopy, Fiber Crete (Dry) 50
Table 3.4 Physical Data for Gamma Spectropscopy, Cured fiber Crete (Industrial Water Added) 50
Table 3.5 Physical Data for Gamma Spectropscopy, U1a Industrial Water 50
Table 3.6 Selected Radionuclides from Gamma Spectroscopy of Native Materials (First Round Sampling 52
Table 3.7 Selected Radionuclides from Gamma Spectroscopy of Native Materials at In-Situ Sampling Location 53
Table 3.8 Selected Radionuclides from Gamma Spectroscopy of Fiber Crete 54
Table 3.9 Selected Radionuclides from Gamma Spectroscopy of Cured Fiber Crete with Industrial Water 55
Table 3.10 Selected Radionuclides from Gamma Spectroscopy, Industrial Water 56
Table 3.11 The Calculated Activity of Radon from its Progeny: Gamma Spectroscopy of Native Materials (First Round Sampling) 56
Table 3.12 Statistics of Native Material Gamma Spectroscopy for Radon Calculations (First round Sampling) 57
Table 3.13 The Calculated Activity of Radon from its Progeny: Gamma Spectroscopy of Native Material Samples from In-Situ Sampling Locations 57
Table 3.14 Statistics of Native Materials (for In-Situ Sampling) Gamma Spectroscopy 58
Table 3.15 The Calculated Activity of Radon from its Progeny: Gamma Spectroscopy of Fiber Crete Samples – Dry 58
Table 3.16 Statistics of dry Fiber Crete Gamma Spectroscopy 59
Table 3.17 The Calculated Activity of Radon from its Progeny: Gamma Spectroscopy of Fiber Crete Samples Cured Material – Uncorrected Activity 59

Reproduced with permission of the copyright owner. Further reproduction prohibited without permission.

Table 3.18 Statistics of Cured Fiber Crete Gamma Spectroscopy (Uncorrected Activity) 60
Table 3.19 The Calculated Activity of Radon from its Progeny: Gamma Spectroscopy of Fiber Crete Samples Cured Material – Corrected Activity 60
Table 3.20 Statistics of Cured Fiber Crete Gamma Spectroscopy (Corrected Activity) 61
Table 3.21 A Comparison of Physical Data of Pre and Post Cure Fiber Crete Samples 61
Table 3.22 Lucas Cell Information for Native Materials Emanation Coefficient Determination 66
Table 3.23 Results of Lucas Cell Analysis for Native Material Emanation Coefficient 66
Table 3.24 Lucas Cell Information for Cured Fiber Crete Emanation Coefficient Determination 67
Table 3.25 Results of Lucas Cell Analysis for Cured Fiber Crete Emanation Coefficient 67
Table 3.26 Lucas Cell Information for Dry Fiber Crete Emanation Coefficient Determination 68
Table 3.27 Results of Lucas Cell Analysis for Fiber Crete (Dry) Emanation Coefficient 68
Table 3.28 In-Situ Passive Diffusion Charcoal Canister Results: First Round Sampling (Native Material) 71
Table 3.29 In-Situ Passive Diffusion Charcoal Canister Results: First Round Sampling (Fiber Crete) 72
Table 3.30 Passive Diffusion Charcoal Canister Statistics: First Round Sampling 73
Table 3.31 Passive Diffusion Charcoal Canister Statistics: First Round Sampling 74
Table 3.32 Passive Diffusion Charcoal Canister Results t-Test 75
Table 3.33 In-Situ Passive Diffusion Charcoal Canister Results (Native Material Surfaces) Second Round Sampling 76
Table 3.34 In-Situ Passive Diffusion Charcoal Canister Results (Fiber Crete Surfaces) Second Round Sampling 76
Table 3.35 Passive Diffusion Charcoal Canister Statistics: Second Round Sampling .. 77
Table 3.36 Passive Diffusion Charcoal Canister Statistics: Second Round Sampling .. 78
Table 3.37 Passive Diffusion Charcoal Canister Results t-Test 79
Table 4.1 Particle Size Distribution 95
Table 4.2 Average Exhalation Values for First Round Sampling 100
Table 4.3 Average Exhalation Values for Second Round Sampling 100

Reproduced with permission of the copyright owner. Further reproduction prohibited without permission.

ACKNOWLEDGMENTS

I am indebted to many individuals and organizations for their cooperation and help, for without their involvement, this study would not have been possible.

First and foremost, a deep appreciation needs to be extended to the UNLV Health Physics Department, specifically my advisor, Dr. William Johnson, who let me run with loose reins but was always accessible when guidance was necessary. In addition, a note of gratitude is given to Dr. Mark Rudin, for his decision to accept me into the Health Physics Masters program, based on, what he saw, was a candidate who could successfully accomplish the established objectives on this program.

Julie Carpenter, the Environmental, Safety and Health Manager for the Los Alamos National Laboratory at the Nevada Test Site, supported this project by allowing access to the U1a Complex and providing the photographs of the underground operations associated with this study. In addition, Ms. Carpenter opened many doors so that the necessary cooperation was extended to me during in-situ collection.

The U1a Complex management, namely Randy Mackey, the U1a Construction Manager and James Foley, the U1a Complex Safety Representative, were more than instrumental in coordinating assistance from the craft personnel, who, in their own right, were tremendous in constructing a sampling area, thus enabling in-situ sampling to be conducted.

Reproduced with permission of the copyright owner. Further reproduction prohibited without permission.

A special note of appreciation to Emilio Braganza and the Environmental Protection Agency and Steven MacLemore of Anteon Corporation (EPA contractor), located on the campus of the University of Nevada, Las Vegas, for their expertise in radon sampling and help in charcoal canister analysis and supplying passive diffusion barrier charcoal canisters for this experiment.

Deep appreciation goes to Joseph Huthinson, chemist for Bechtel Nevada at the Nevada Test Site who gave genuine, selfless help, support and time towards lucas cell theory and analysis.

Lastly, thank you to Nick Nicholson and the QUIKRETE Companies, for giving permission to mention their product, "concrete mix 1101 (AKA fiber crete)" which was the focal point of this entire study.

Reproduced with permission of the copyright owner. Further reproduction prohibited without permission.

CHAPTER I

INTRODUCTION

1.1 Occupational and Non-Occupational Radon Exposures

The health effects of radon gas first drew national attention in December, 1984, when a contractor engineer at the Limerick Generating Station in Pennsylvania was detected with extremely high radiation contamination. Initially this was believed to be the result of a personal occupational exposure. After an extensive investigation, it was discovered that the high readings were due to radon and radon daughters originating from the engineer's house. Since that time, studies, such as those compiled by the International Council of Radiation Protection (ICRP) and the National Council of Radiation Protection and Measurements (NCRP), have correlated radon gas with adverse health effects within underground environments as well as in office buildings and residential homes (ICRP 1994 and NCRP 1987). Current indoor air quality studies for such environments indicate that building materials, such as brick and concrete, are main constituents for radon exposure (ICRP 1987). Studies conducted in the United States, United Kingdom, Germany, and Sweden, have quantified airborne radon concentrations originating from these materials to range from 0.7 - 100 Becqurels per meter cubed (Bq m^{-3}) (ICRP 1987). Current estimates have placed radon-attributed lung-cancer deaths in the United States at 15,400 - 21,800 per year (National Research Council 1999).

Reproduced with permission of the copyright owner. Further reproduction prohibited without permission.

Many studies have focused on persons working in underground environments, with great attention to uranium miners. Radionuclides, indigenous to the native lithology, have been quantified and used to determine potential health problems. At the same time, many materials used in underground construction, and similar to those identified in indoor air quality studies, have not been considered as potential contributing factors. Typically, during mining operations or underground construction, cementaceous materials, such as fiber-crete or shot-crete, are used to solidify the sides (ribs) and ceilings (backs) of underground mines and tunnels. Many times cement is poured on the floor decking (invert). These types of materials can be made by either indigenous aggregate substances or manufactured in batch at plants distances from the end-use site. Depending on where these construction materials are quarried, the amount and types of radionuclides can vary, modifying the exposure of workers to radioactivity within the work environment.

While construction materials may contain naturally occurring radioactive materials (NORM), their effect on humans may or may not warrant concerns, as their natural radioactivity may be different from the native soils to which they support. In addition, underground construction materials may also act as a shield for native material radionuclides. On the other hand, these construction materials may increase underground exposures due to their potential to increase airborne radioactivty. This report focuses on how one specific underground construction material, fiber crete, contributes to the quantity of one NORM radionuclide, radon-222, within an underground environment.

Reproduced with permission of the copyright owner. Further reproduction prohibited without permission.

1.2 Properties of Radon

Radon - 222 has an atomic number of 86, with an atomic weight of 222. It is a noble gas that is colorless. It's density is 9.72 grams l^{-1} (air has a density of 1.29 grams l^{-1}).

Radon (^{222}Rn) is the decay product of radium (^{226}Ra), which is part of the ^{238}U decay series. ^{226}Ra decays to ^{222}Rn with approximately 95% of its released energy being alpha emission and approximately 4% released by gamma emission (0.186 MeV). The half-life for ^{226}Ra is 1620 years (Shlein 1998). ^{222}Rn has a half-life of 3.8235 days, which is the longest of any of its sister isotopes, ^{220}Rn (thoron) and ^{219}Rn, with half-lives of 55.61 seconds and 3.96 seconds, respectively. ^{220}Rn is a result of the thorium decay chain (beginning with ^{232}Th), while ^{219}Rn is a decay product from the actinium series, beginning with ^{235}U. All three radon isotopes decay via alpha emission. The prime decay products of ^{222}Rn are ^{218}Po, ^{214}Pb, ^{214}Bi, ^{214}Po, ^{210}Pb, and ^{210}Po, reaching stability with ^{206}Pb.

From a historical point-of-view, the first association between radon exposure and health effects was in the sixteenth century. Paracelsus (1494 - 1541), considered by many to be the father of toxicology, noted unusually high mortalities from lung disease among persons working in the silver mines of Schneeberg, Saxony (what is now Germany). The same phenomenon was noted by the sixteenth century physician, Agricola, at the mines in Joachimstahl (now Jachymov, Slovokia). While Agricola documented that the silver ore in Joachimstahl was mined near the surface, mining at Schneeberg occurred at depths of almost 400 meters (ICRP 1994). Paracelsus named the *Schneeberg*

Reproduced with permission of the copyright owner. Further reproduction prohibited without permission.

lungenkrankheit (Schneeberg lung disease) as "mala metallorum." (Hoover 1950). The frequency of the affliction increased at Schneeberg in the 17^{th} and 18^{th} centuries as the mining of silver, cobalt and copper increased.

It was not until the nineteenth century that Paracelsus's *Schneeberg lungenkrankheit* was identified as lung cancer (ICRP 1994). The persons responsible for this identification, Haerting and Hesse, estimated that 75% of the miners in the Schneeberg region died of lung cancer. (ICRP 1977). In 1924, it was suggested that these cancers were attributed to radon exposure by Ludewig and Lorenser (ICRP 1994). The specific association between observed high lung cancer incidence and radon emanating from radium-bearing rocks in these same regions, was established in the 1950's (Bale 1980). During this same period, it was established that the causative agent was actually radon daughters, as opposed to radon gas itself (Bale and Shapiro 1956).

From the 1800's to the early 1900's, approximately 400 lung cancer deaths were recorded in the Schneeberg mining industry. The average radon level in the mining air was estimated to be 2900 pCi l^{-1} (Lao 1990). Radon daughter levels were estimated to be between 10 - 180 working levels (WLs): a term that will be explained, in detail, later on in this paper. Between 1929 - 1940, autopsy reports showed about 50% of the deaths among Joachimsthal miners were from lung cancers (NRC 1991). The radon levels were reported to be similar to those estimated in the Schneeberg Mines.

The initial parent material of radon, uranium, makes up approximately 3 parts per million (ppm) of the earth's crust (ICRP 1977). Consequently radon can be found throughout the world, in varying concentrations, with the higher airborne concentrations, found naturally, in underground cavities. Concentrated deposits of uranium (known as

Reproduced with permission of the copyright owner. Further reproduction prohibited without permission.

ores) are found in a few places, typically located in hard rock or sandstone and mined in the southwest United States, Australia, parts of Europe, Namibia, South Africa, Niger and Canada. The world's largest deposits have been found in the Canadian province of Saskatchewan. Uranium is also found adsorbed in phosphate materials (NCRP 1987), where, in the United States, three areas have been identified with elevated concentrations: Southeastern Idaho and neighboring parts of Montana, Wyoming, Utah, and Nevada (350,000 km^2), Central Florida (2600 km^2), and Central Tennessee and Northern Alabama (2800 km^2). In addition, the Colorado Plateau has been identified with substantial uranium deposits, although not due to adsorption within phosphates (NCRP 1987).

Due to radon's inert properties, once formed in radium-bearing materials, radon atoms are relatively free to move without bonding with other elements or molecules. This improves their ability to transfer through the materials' pores. Therefore, radon can reach air or water with relative ease and can then come into contact with humans. The 3.8 day half-life is long enough that much of the ^{222}Rn formed within radium-bearing materials (or native soils) within a depth of one meter can reach the breathing air environment (Nazaroff and Nero1988). The short-lived progeny interact with materials, such as human tissue, by electrostatic or chemical mechanisms. This results in energy being released within the materials that the progeny come into contact. Four of radon's progeny have half lives of less than 30 minutes, and therefore, if deposited in the lung (upon inhalation), are likely to decay to ^{210}Pb (22.3 year half life) prior to being removed by lung clearance mechanisms (Nazaroff and Nero 1988).

Reproduced with permission of the copyright owner. Further reproduction prohibited without permission.

The radiation released upon decay of the short-lived progeny results in a lung dose to which increased lung cancer is attributed. The alpha emission from the polonium isotopes (^{218}Po and ^{214}Po) contributes significantly to this risk primarily because the alpha particles deposit their energy within the thin tissue layer of the respiratory system bronchioles. Therefore, the alpha energy is deposited in the sensitive lung tissue with a relatively dense deposition pattern, resulting in a biological impact (Nazaroff and Nero 1988).

1.3 Emanation Coefficients

Measurement of radon in the native soil and underground construction materials cannot be used, as the sole indicator, to determine their influences on radon exposure within a given environment. A major factor that influences the amount of radon released from the radium-bearing native soil into the atmosphere, and resulting in the potential human exposure, is the phenomenon known as emanation. Emanation power, or "coefficient of emanation" is defined as the ratio of the number of radon atoms that escape from a quantity of material to the total number of atoms formed by the radioactive decay of radium in the material.

Table 1.1 is a compilation of individual studies displaying the ^{222}Rn emanation coefficients for various natural materials. This table shows that emanation coefficients for soils can vary from 0.02 - 0.7, depending on soil type (Nazaroff and Nero 1988), while soil porosity and moisture content appear to be major factors. For instance, while soils, in general, have been measured with an average emanation coefficient of 0.30, a soil that has been dried at 90° C for 200 hours has a coefficient of 0.09, and the same soil,

Reproduced with permission of the copyright owner. Further reproduction prohibited without permission.

Table 1.1: Measurements of ^{222}Rn Emanation Coefficients

Material	# Samples	Moisture Content	Emanation Coefficient[a]
Crushed Rock	58	Unknown	0.084
Soil	21	Unknown	0.30
Soil (20 μm mesh)	1	Dried @ 105 °C (24 hours)	0.25
Soil	1	20% of dry weight	0.68
Soil	1	Same as above, dried at 200° C (90 hours)	0.09
Soil	2	13 - 20% of dry weight	0.27
Sand	7	Unknown	0.14
Sand	1	Saturated	0.24
Sandy Loam	7	Unknown	0.21
Silty Loam	7	Unknown	0.24
Heavy Loam	12	Unknown	0.20
Clay	5	Unknown	0.28

Source: Nazaroff and Nero 1988

a = Emanation Coefficients are based on an arithmetic mean

Reproduced with permission of the copyright owner. Further reproduction prohibited without permission.

having a moisture content of 20% of the material dry weight, has a coefficient of 0.68. The Hawaiian soils also show variations in emanation coefficients that appear to be moisture influenced. Lava field soils were measured with a coefficient of 0.02; much lower than the coefficient for thin organic soils (0.55) or deep agricultural soils (0.70). While Table 1.1 specifies the moisture content for these soils to be "unknown," it would stand to reason that deep agricultural soils would have a high moisture, especially when compared to lava field soils. A comparison of sands show an increase in emanation coefficients from 0.14 to 0.24 for unknown moisture content to the point of saturation, respectively. It is assumed that the unknown moisture content would be less than saturated. This influence of moisture on radon emanation can be explained from radon's hydroscopic (moisture affinity) property. Therefore, soils with high moisture content can attract radon gas from the soil medium (Kathren 1984) causing radon gas to be extracted from its host material.

Strong and Levins studied the effect of moisture content for radon emanation with uranium ore and uranium tailings. The results show that as moisture content increases, the emanation coefficient increases. At the water saturation limit, the emanation coefficient reaches its maximum value (Strong 1982).

Particle size also influences radon emanation. A comparison of finer particle size materials, such as clays and silty loams were measured to have coefficients of 0.28 and 0.24. These numbers are slightly higher than those for sandy and heavy loams, measured at 0.21 and 0.20. Crushed rock (at variable moisture content) has an emanation coefficient ranging from 0.005 - 0.40. In addition to natural rocks and soils, building

Reproduced with permission of the copyright owner. Further reproduction prohibited without permission.

materials also have radon emanation factors. Table 1.2 lists the emanation coefficients for some popular building materials.

When ^{222}Rn atoms are created (from the alpha decay of ^{226}Ra), they posses 80 keV of kinetic energy (Nazaroff and Nero 1988). The newly formed atom travels from the point of origin until its energy has been transferred to its host material. The distance traveled depends on the density and composition of the material. For common solid materials, ^{222}Rn travels 0.02 - 0.07 μm, for water: 0.1μm, and for air: 63 μm (Nazaroff and Nero 1988).

There are three general modes of operation for which radon atoms can leave their host (i.e. radium-bearing) material: direct recoil, indirect recoil, and diffusion (NCRP 1988). These components are classified on the basis of the locations of the end points of the path of the recoiling atoms. Direct recoil refers to radon atoms that terminate their recoil in the fluid-filled pore space. Indirect recoil refers to atoms that leave the grain and penetrate another grain. Diffusion refers to radon atoms that begin and end their recoil within a single grain, then migrate to the pore through molecular diffusion. While all three transfer modes have been observed, measurements of the fraction diffusing out of the atom have been noted to be negligible (Nazaroff and Nero 1988). Many observations indicate that actual radon emanations are greater than the theoretically calculated travel distances. Two theories have been offered. One suggests a non-uniformity in radium deposition with concentrations along secondary crusts or films on the grain surfaces. A second explanation suggests that chemical corrosion and radiation damage from radon precursors damages the grain's crystalline structure in the vicinity of newly formed

Reproduced with permission of the copyright owner. Further reproduction prohibited without permission.

Table 1.2: Emanation Coefficients of Some Building Materials

Material	Emanation Coefficient
Concrete	0.1 - 0.4
Brick	0.02 - 0.1
Gypsum	0.03 - 0.2
Cement	0.02 - 0.05
Fly Ash	0.002 - 0.02

Source: Pensko and Stpiczynska, 1980

Reproduced with permission of the copyright owner. Further reproduction prohibited without permission.

^{222}Rn, and thereby permit radon to migrate more readily than what would appear to be theoretically possible.

The size of the individual grains that host individual radon atoms can also play an influence on emanation. Individual radon atoms need a higher recoil energy to escape larger host grains.

Previous studies indicate that the release of radon from soil is at a maximum when the soil is moist (Nazaroff and Nero 1988). This is due to a shorter recoil range in water than in air. Therefore when a radon atom enters a pore that is partially filled with water, it has a very high probability to terminate its recoil in water. At this point, the radon atom is readily transferred to the air in the pore.

Based on radon's recoil in water and subsequent transport to air, pores filled with water result in a higher radon emanation coefficient. Therefore, a radon atom entering a pore that is slightly filled with water has a very high probability of terminating its recoil in the water, and, once in the water, radon atoms can be readily transferred to the air in the pore. This is supported by Henry's Law, which shows a rapid transport of gas from water to air under normal temperature and pressure conditions (Nazaroff and Nero 1988). Even when pore size increases (within water-filled pores), radon transport is reduced only slightly. This suggests that moisture exerts a greater influence on radon emanation then the influence of pore size.

While studies do not indicate a strong correlation between temperature and emanation coefficients, there is evidence which indicates that a proportional relationship does exist. This has been attributed to observations that indicate a temperature increase causes a reduction in physical adsorption by the surrounding grains, resulting in an

Reproduced with permission of the copyright owner. Further reproduction prohibited without permission.

increase in radon flux . While temperature has been shown to effect radon emanation, studies involving the common temperature ranges in soils have indicated only minor significance (Strandon 1984). Significant changes in emanation coefficients have been observed (from 0.106 decreasing to 0.081) when temperatures changed from 265°C to -20°C (Barretto 1973). It was further shown that as temperatures became colder, emanation coefficients continued to decrease. However, these temperature differences used to observe such changes in the emanation coefficients, are much greater than what typically occurs in an underground environment.

While temperature itself does not play such a significant role as moisture in diffusion transport, the speed of diffusion is directly effected by temperature. The equation below shows the diffusion coefficient (used in Fick's law of diffusion), expressed in terms of a particular gas's properties.

$$D_a = 2\left(3\Pi^{3/2} d^2 P\right)^{-1} \left(\kappa^3 T^3 m^{-1/2}\right)^{1/2} \qquad (1.1)$$

Where:

D_a = Diffusion Coefficient

κ = Boltzmann constant (1.38×10^{-16} ergs K^{-1})

P = Pressure

T = Temperature

d = distance

m = mass

Fick's second law of diffusion relates the actual concentration gradient to the diffusion coefficient.

Reproduced with permission of the copyright owner. Further reproduction prohibited without permission.

$$(dC_a)(dt)^{-1} = (D_a)\nabla^2 C_a \qquad (1.2)$$

Where:

$(dC_a)(dt)^{-1}$ = Concentration gradient

D_a = Diffusion coefficient

∇ = Three-dimensional gradient operator

C_a = Concentration of substance "a"

Equation 1.2 shows that the relationship between the diffusion coefficient and concentration gradient is directly proportional to each other. Therefore, based on these two equations, it can be concluded that a gas's diffusivity is not only directly proportional to its concentration gradient, but also the system temperature.

1.4 Exhalation

The transfer of radon across the interface between a solid phase and the atmosphere is often referred to as exhalation or radon flux. Exhalation differs from emanation as exhalation includes the emanation factor (whereas radon is emanated from solid grains to the pore spaces between the grains or into the water surrounding the grains), plus the transport of radon into the atmosphere via concentration or pressure gradients. Table 1.3 lists exhalation rates of a few common materials.

The entry rate of radon gas from soils to the ambient free air strongly depends on a number of factors, including soil permeability, surface cracks, pressure differences differentiation. The average radon concentration in the soil gas has been estimated to be about 1000 times higher than in the free ambient air environment at sea level (ICRP 1987). Therefore, if radon transport does occur, high radon concentrations in the ambient air is a strong possibility.

Reproduced with permission of the copyright owner. Further reproduction prohibited without permission.

Table 1.3: Radon Exhalation Rates of Some Building Materials

Material	Exhalation Rate (Bq hr^{-1} m^{-2})
Concrete	2 - 30
Brick	2 - 5
Alum Shale Concrete	50 - 200
By-Product Gypsum	5 - 40
Lightweight Concrete	1 -3

Source: Nazaroff and Nero, 1988

Reproduced with permission of the copyright owner. Further reproduction prohibited without permission.

Atmospheric pressure and humidity have been observed as having strong influences on radon exhalation (Nazaroff and Nero 1988). McLaughlin and Jonassen observed sudden pressure drops resulting in increased radon exhalation in building materials (McLaughlin and Jonassen 1980). Studies in uranium mines show evidence of a correlation between barometric pressure and radon exhalation rates. Musulin, Franklin and Thomas (1982) showed that a positive correlation exists between ventilation and radon exhalation rates, whereas airborne radon concentrations increased when the underground ventilation system was turned off , reaching a maximum steady state concentration. The concentration decreased when the ventilation system was turned back on, reaching a minimum steady state concentration.

Similar to emanation coefficient, moisture also influences radon exhalation. To date, studies have indicated conflicting data as far as how exhalation rates are influenced. Indoor air studies in high rise buildings have indicated that as concrete construction materials age and the moisture content decreases, the exhalation rate is reduced (Yu, Chan, and Young 1995). Studies by Strandon and Kolstad have demonstrated that the exhalation factor may vary by as much as a factor of 20 as the material's moisture content changes. However, contrary to Yu, et al, the exhalation rate was observed to increase as the moisture content increased (Strandon and Kolstad 1984).

Rogers, Nielson and Holt (1995) described the increase in exhalation rates of aged concrete as the result of an increased permeability and diffusivity. A rapid increase in exhalation occurred in the first 12 years at the same time as the material's permeability increased. This increase gradually slowed down until a maximum permeability was

Reproduced with permission of the copyright owner. Further reproduction prohibited without permission.

reached at 20 years. This was followed by a decrease in permeability and radon exhalation rates.

Snoddy (1995) in his study of "Permeability and Diffusivity Characteristics in Florida Concretes," was able to draw a positive relationship between the amount of water within concrete and its permeability and diffusivity coefficients. This could explain the increased radon exhalation rates with increased moisture observed by Rogers et al.

1.5 Radon and Radon Progeny

The recognition of radon and radon progeny as contributors to lung cancer in uranium miners lead to limitation guidelines as early as 1940 (Evans and Goodman 1940), where a safety factor of 100 was applied to the estimated levels believed to be representative of the exposures in Joachimsthal, Czechoslovakia. This guideline was established at 10 pCi l^{-1} of radon (ICRP 1977).

In Salt Lake City, Utah, February, 1956, an organization called the Seven States Mining Conference adopted a maximum permissible concentration for radon (in equilibrium with radon daughters) of 100 pCi l^{-1}, which is equivalent to 370 kBq m^{-3}, referring to it as a "working level" (WL). Because the degree of equilibrium between radon and its short lived daughters was rarely known, the United States Public Health Service, in 1957, redefined WL in terms of alpha energy released by the decay of radon daughters, which, in turn, could be directly related to the dose delivered to the lungs (Kathren 1984). Today WL is defined as any combination of short-lived radon daughters (^{218}Po, ^{214}Pb, and ^{214}Bi) in air that will result in the ultimate emission of 1.3 x 10^5 (MeV) of alpha particle energy. This value is equal to the initial WL established in 1956 of 100

Reproduced with permission of the copyright owner. Further reproduction prohibited without permission.

pCi l^{-1}, assuming all progeny are in equilibrium. The combination of radon progeny is not taken into account with this WL definition. Therefore, the modern WL definition is independent of the degree of equilibrium or combination of any one nuclide in the radon decay chain (Kathren 1984).

Under typical equilibrium conditions, a radon concentration of 1 pCi L^{-1} translates to approximately 0.005 WL (NRC 1991). In international (SI) units, the activity of radon per unit mass of air is expressed in units of Bq m^{-3}. At equilibrium between radon and its progeny, 1 WL corresponds to 3.7 x 10^5 Bq m^{-3} (NRC 1991).

A term defined from WL is working level month (WLM). WLM was developed to describe the exposure to radon progeny in underground mines (Holaday 1957). The WLM is based on an airborne concentration of radon progeny of one WL for a typical working month of 170 hours. It is equal to 3.5 x 10^{-3} mJ h m^{-3}. Therefore, an underground worker who is exposed to a radon progeny concentration of 1.3 x 10^5 MeV l^{-1} for 170 hours, would have an exposure of 1 WLM. Workers exposed to four times this concentration in a 170 hour work period, would receive an exposure of 4 WLMs. This would be approximately the same exposure in a residential environment with an airborne concentration of 1 WL. This is due to the fact that approximately four times the amount of time is spent in a non-work setting when compared to a typical 170-hour work month. Therefore, an adult spending 60% of the time in a home with a concentration of 1 WL would receive an exposure of 2.4 WLMs (0.6 x 4 WLMs).

In 1981, the International Commission for Radiation Protection (ICRP) recommended that the annual limit for the effective dose equivalent of 0.05 seiverts

Reproduced with permission of the copyright owner. Further reproduction prohibited without permission.

(equivalent to 5 rem) should be applied to miners that are exposed to radon and its progeny (ICRP 1981). As a result, the ICRP recommended an anuual limit of intake (ALI) for any mixture of alpha-emitting radon progeny of 0.02 joules. This intake is based on the maximum unattached radon progeny fraction of 0.05 with an average breathing rate of 1.2 $m^3 hr^{-1}$. This equates to an ALI of 4.8 WLMs and a derived airborne concentration (DAC) of 0.4 WLs. All DACs are based on a 2000 hour working year. This exposure limit corresponds to a radon activity concentration that is in equilibrium with its short-lived progeny that would have the same potential alpha energy concentration as the existing non-equilibrium mixture of 1500 Bq m^{-3} (ICRP 1994).

For ^{222}Rn alone (without any progeny taken into account), the ICRP recommended an annual limiting exposure of 3 x 10^8 Bq h m^{-3} (ICRP 1981). The recommended DAC was 1.5 x 10^5 Bq m^{-3}. The current legal occupational exposure limit for ^{222}Rn without progeny is 1 x 10^4 μCi (ALI) or 1.5 x 10^5 Bq h m^{-3} and 4.0 x 10^{-6} μCi · ml^{-1} (DAC) or 1.5 x 10^5 Bq m^{-3}, while the ALI for ^{222}Rn in equilibrium with its progeny is 1 x 10^2 μCi (ALI) or 1500 Bq-h-m^{-3} with a DAC of 3.0 x 10^{-8} μC ml^{-1} or 1000 Bq m^{-3} (US NRC 1992).

1.6 Natural Radioactivity in Materials

The abundance of parent radionuclides, specifically ^{238}U and ^{226}Ra, within construction materials depends upon their natural concentrations in the source rock and fiber crete. General "rules-of-thumb" are provided in NCRP reports which summarizes the major nuclides in various rock types. A typical value of ^{226}Ra in crustal rock is 0.040 Bq g^{-1}, while for concrete materials, ^{226}Ra has been typically measured at 0.030 – 0.070

Reproduced with permission of the copyright owner. Further reproduction prohibited without permission.

Bq g^{-1} (NCRP 1988). These activities should be similar for ^{222}Rn as equilibrium between ^{226}Ra and ^{222}Rn is achieved in a few weeks.

Table 1.4 illustrates typical concentrations of ^{226}Ra in various rock types. By assuming an equilibrium condition exists between ^{226}Ra and ^{222}Rn within the Ula native material, gamma spectroscopy results can be compared to typical ^{226}Ra activities as a way to verify the detected activities.

While radionuclides may be present in native and construction materials, how they contribute to radon exposure is dependent on many factors. Factors that directly influence the flow of radon atoms from soil to air are:

1. Concentration of parent (^{226}Ra) in materials
2. Emanation power of ^{222}Rn
3. Porosity of the materials
4. Atmospheric pressure differentials across the interface
5. Degree of water saturation

By measuring the radon flux (exhalation), which is the transfer of radon across the interface between a solid phase and the atmosphere, the radon contribution of construction materials can be determined. Taking various measurements at pre-determined underground locations, with and without construction materials, comparisons can be made. NCRP (1988) states the radon flux for 21 different US sites average 20 mBq $m^{-2}s^{-1}$ (3.33 Bq $cm^{-2}hr^{-1}$), with a range of 2 - 50 mBq $m^{-2}s^{-1}$ or 0.33 - 8.33 Bq cm^{-2} hr^{-1}. These numbers are similar to those exhalation rates listed in Table 1.3.

Reproduced with permission of the copyright owner. Further reproduction prohibited without permission.

Table 1.4: ^{226}Ra Concentrations in Various Types of Rocks

Rock Class	Example	# Samples	^{226}Ra Average Activity ($Bg\ kg^{-1}$)	^{226}Ra Activity Range ($Bg\ kg^{-1}$)
Acid Extrusives	Rhyolite	131	71	10 - 285
Carbonates	Limestone	141	25	0.4 - 223
Clay	N/A	40	50	14 - 198
Sandstone and Conglomerate	N/A	198	51	1 - 770
Chemical Sedimentary Rocks[a]	Evaporates	243	45	0.4 - 335
Detrital Sedimentary Rocks[b]	N/A	412	60	1 - 992
Basic Extrusives	Basalt	77	11	0.4 - 41

Source: Nazaroff and Nero 1988

a: Includes carbonates
b: Includes clay, shale, sandstone, and conglomerates

Reproduced with permission of the copyright owner. Further reproduction prohibited without permission.

The average radon flux from soil in the U.S. to air has been estimated at 17 mBq $m^{-2}s^{-1}$ and has been mostly attributed to diffusion (NCRP 1988). While building materials are quite variable, studies indicate that the exhalation rates are mostly lower than those observed in soils. This suggests that construction materials in underground environments may reduce the radon exhalation from native soils while contributing radon concentrations due to their own exhalation abilities. Since previous studies have estimated lower exhalation rates for construction materials, the overall radon concentration would be less, resulting in a reduced exposure to underground workers.

NCRP 97 (NCRP 1988) lists five methods (classified by the National Bureau of Standards) used for measuring exhalation. These methods are:

1. Accumulation method
2. Flow method
3. Adsorption method
4. Vertical profile method
5. Soil concentration gradient method

This thesis considers two of these methods, accumulation and adsorption, as they appear to be the most practical method to collect radon gas as it exhales through the underground surfaces and into the working drifts. The accumulation method is the earliest method. It consists of sealing the open end of a vessel to the surface being measured. The radon concentration inside the vessel is measured, usually by an alpha scintillation counter. One of the difficulties applying this technique is being able to have a tight seal between the vessel and the rough underground surfaces. Another problem exists with the possibility of creating an artificial pressure differential between the native soils and the

Reproduced with permission of the copyright owner. Further reproduction prohibited without permission.

accumulation vessel which requires a pump to draw exhalated radon into the unit. This artificial pressure differential may force more radon out of the native soils than what would be occurring under typical conditions, thereby creating inflated results.

The adsorption method appears to be the more feasible of the two sampling modes as radon gas is easily adsorbed by the capture media (charcoal) and does not rely on any pump to assist in radon capture. However; creating a proper seal between the underground surface and collection canister will still be a concern. Detection is accomplished by gamma spectroscopy, based on the radon progeny, ^{214}Pb and ^{214}Bi, having major gamma energy peaks at 0.242, 0.295, and 0.352 MeV (^{214}Pb) and 0.609, 1.120, 1.764, and 2.204 MeV (^{214}Bi) (Kocher 1981). More will be discussed about this method in the "Methods and Materials" section of this report.

1.7 Hypothesis

This paper is a study, to determine whether construction materials influence the amount of radon gas that naturally exhalates through underground surfaces and into the work areas. The research hypothesis for this study is that construction materials (i.e. fiber crete) used in underground environments to support underground surfaces, influence the radon concentration emanating from the surrounding native materials. The null hypothesis states that the fiber crete in an underground environment does not influence the amount of radon emanating from the surrounding native materials and into the underground setting. Alternative hypotheses would be that the fiber crete either increases or decreases the amount of radon emanating from the surrounding native materials. This may be because radon from the fiber crete itself may influence airborne concentrations, or

Reproduced with permission of the copyright owner. Further reproduction prohibited without permission.

the fiber crete materials may act as a shield for the radon gas exhalating from the native materials.

While, results may support the null hypothesis, it cannot be concluded that the construction materials examined in this study do not influence radon exhalation, only that an influence was not observed. In this respect, data may be misinterpreted as the specific thickness, or density of the fiber crete may shield the same amount of activity to which it contributes. Therefore, by definition, the null hypothesis can never be proven; only that the research and alternative hypotheses were not proven, based on the specific setting and collected data.

Reproduced with permission of the copyright owner. Further reproduction prohibited without permission.

CHAPTER II

METHODS AND MATERIALS

2.1 The U1a Complex

The site studied in the work was the U1a Complex, located in Area 1 of the Nevada Test Site (NTS), Nye County, Nevada. This site was selected because of concerns have been expressed regarding radon gas exposures to underground workers and the effects imposed by the construction materials used to support the actual facility.

The U1a Complex is approximately 962 feet below ground level and 600 feet above the existing water table (Smith et al., 1998). Figure 2.1 illustrates this underground facility with the specific area where sample collection and in-site measurements were conducted, known as the .05 drift. The complex itself, is situated in an internally draining, alluvium filled arid basin. The alluvium is estimated to be 1800 feet thick and rests on tertiary volcanic rock (Allen, 1996). This facility's current purpose is to support the United States Nuclear Stockpile Stewardship Program, where national laboratories conduct experiments involving sub-critical reactions.

The NTS encompasses an approximately rectangular area 50 miles North to South and 30 miles East to West within a region of generally North-South trending ridges and valleys in Southern Nevada. The terrain is extremely irregular, with elevations ranging

Reproduced with permission of the copyright owner. Further reproduction prohibited without permission.

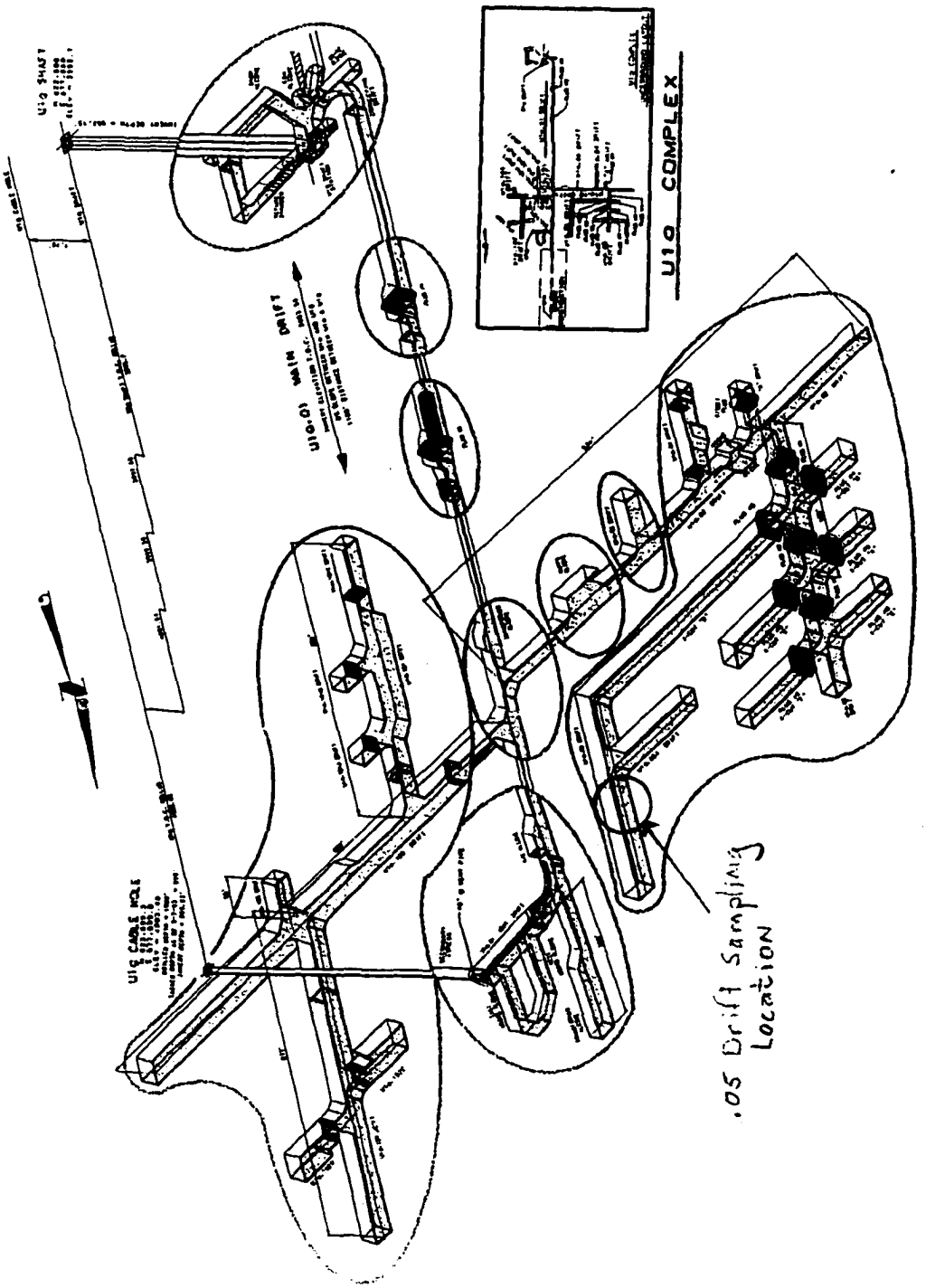

Figure 2.1 U1a Complex

Reproduced with permission of the copyright owner. Further reproduction prohibited without permission.

from 7,700 feet above mean sea level (MSL) on Rainier Mesa in the North to 3,100 feet above MSL in Frenchman Flat (i.e. area surrounding Frenchman lake) in the Southeast and 2,700 feet above MSL in the extreme Southwest corner on the edge of the Amargosa Desert. Elevations of the basins within the NTS range from 5,344 feet above MSL in the mountains to the Northwest to 3,477 feet above MSL adjacent to Mercury Highway. There is a general, but frequently interrupted, downward slope from North to South (Quiring, 1968).

The U1a Complex is located within the East central portion of the NTS, approximately 5 miles North of Control Point-One (CP-1) in Area 1 and approximately 27 miles North of Mercury, Nevada.

The NTS is operated by the United States Department of Energy (U.S. DOE), and managed by a privately-owed contractor, Bechtel Nevada (BN). The facility itself is the responsibility of the Los Alamos National Laboratory (LANL), while maintenance and construction activities are conducted by BN. Additionally, while LANL maintains the overall responsibility of the U1a Complex, there is an agreement that other national laboratories may also use the U1a Complex.

2.2 Regional and Site Geology

In general, the geology consists of three major rock units. These are: (1) complexly folded and faulted desimentary rocks of Paleozoic age averlain at many places by (2) volcanic tuffs and lavas of Tertiary age, which (in the valleys) are covered by (3) alluvium of late Tertiary and Quaternary age. The sedimentary rocks of Paleozoic age are many thousands of feet thick and are comprised mainly of carbonate rocks (dolomite and limestone) in the upper and lower parts, separated by a middle section of clastic rocks

Reproduced with permission of the copyright owner. Further reproduction prohibited without permission.

(shale and Quartzite). The volcanic rocks in the valleys are down dropped and tilted along steeply dipping normal faults of recent Tertiary age. The alluvium is rarely faulted. Compared to the Paleozoic rocks, the Tertiary rocks are relatively underformed and dips are generally gentle. The alluvium is derived from erosion of the nearby hills of tertiary and Paleozoic rocks (DOE, 1991).

The oldest strata in the vicinity on the NTS consists of a 5,000-foot sequence of Precambrian and lower Cambrian clastic rock overlain by a 15,000-foot sequence of Middle Cambrian to Middle Devonian carbonate rock. This is interspersed by volcanic tuffs and lavas of Tertiary age. The Eleana Formation, 7,800-foot thick Middle Cambrian to Middle Devonian and Mississippi age rock, overlies the lower carbonate sequence. The Eleana formation, in turn, is overlain by a 3,600-foot thick carbonate sequence of Pennsylvania-Peruvian age.

The volcanic rocks of Tertiary age are predominantly tuffs. which erupted from various volcanic centers, and lavas, which are mostly of rhyolitic composition. The aggregate thickness of the volcanic rocks is many thousands of feet, but in most places the total thickness of the section is far less because of erosion or nondeposition. Alluvial materials fill 2,000 to 3,000 feet in the central portions of the valleys. The alluvium in Yucca Flat is vertically offset along the preminent North-South trending Yucca Fault.

Drainage-basin soils are composed of alluvial materials. In accordance with the Unified Soil Classification System developed by the U.S. department of Agriculture (USDA), Soil Conservation Service, these materials are classified as silty sand and are further identified with the group symbols SW-SM. Soils of this type range in permeability from rapid to moderately rapid. As defined in USDA (1985), the soil types

Reproduced with permission of the copyright owner. Further reproduction prohibited without permission.

and vegetative cover prevalent in this vicinity are characteristic of Hydrology Soil, Group B.

Alluvium within the U1a Complex is chiefly moderate-to-poorly sorted clay, silt and gravel. Individual clasts within the alluvium range from clay to small boulder-size, with sand size material making up the bulk of these deposits (Allen, 1996).

Individual grains within the alluvium are subangular to rounded, and exhibit low-to-high sphericity. Individual beds within the alluvium are relatively thin (usually 1 centimeter thick), while displaying similar lithologies, showing interfingered and discontinuous channalization (DOE 1991).

Secondary calcium carbonate is considered ubiquitous in the U1a Complex alluvium, with the most noticeable form being horizontal caliche stringers. These stringers are typically less then one centimeter in length and are comprised of finely laminated carbonate. It has been noted that this lithology directly influences permeability and represent important factors in understanding fluid flow through the alluvium (Allen, 1996).

Representative material samples have been previously collected to characterize carbon dioxide (CO_2) and water (H_2O) content within the native materials, along with grain density, specific gravity and grain size determination. Table 2.1 shows these sample results for various locations throughout the U1a Complex. This information was used to calculate the native material porosity (30.8%), saturation (49.4%), and air voids (15.6%) (Allen 1996).

Reproduced with permission of the copyright owner. Further reproduction prohibited without permission.

Table 2.1: Comparison of Physical Property Results (averages) for U1a Location

Sample Location	Clay (%)	Silt (%)	Sand (%)	Pebble/ Cobble (%)	Grain Density (g/cc)	H_2O Content (%)	CO_2 (wt.%)	Specific Gravity
Ledoux	2.15	6.74	65.47	25.7	2.61	7.2	10.4	N/A
.01 drift	7.8	3.2	67.9	21.2	2.59	9.1	12.2	2.41
.02 drift	5.0	7.0	56.0	31.8	2.63	4.2	15.8	2.55
.01/.02 average	6.4	5.1	62.0	26.5	2.61	5.9	13.6	2.47
.03	8.9	5.6	61.8	23.6	2.56	8.8	------	2.47

----, Values were unreasonably low and may be spurious

Source: Allen, 1996

Reproduced with permission of the copyright owner. Further reproduction prohibited without permission.

The U1a Complex is sited in Quaternary alluvium at the depth of approximately 962 feet. The moderately indurated alluvium is composed of slightly to moderately consolidated fluvial and slope wash deposits of silt, clay, cobbles and boulders. Generally the material is poorly sorted, but some beds are moderately sorted. Beds range in thickness from 0.5 feet to 3 feet. Channel deposits are usually about 3 feet wide by 1 foot to 2 feet thick.

2.3 Mining Application

The U1a Complex consists of a network of drifts (underground horizontal pathways). These drifts are pathways to smaller drifts or chambers, referred to as alcoves, where various experiments are conducted. To meet the continued need of the experiment schedules, additional drifts and alcoves are created. The method employed for the construction of underground expansion is "continuous" mining, in which digging methods are used to remove the in-place native materials. This is an alternative method to "conventional" mining practices that use explosives.

Continuous mining techniques at the U1a Complex involve heavy pieces of electrical equipment called alpine miners which have rotating cutting metal heads (approximately 2 feet diameter metal balls). The cutting heads contain metal carbide tips located uniformly over the entire surface. Each cutting head has 75 cutting bits, each of which is four inches long. Alpine miners are manually operated by a driver located inside the alpine miner with a spotter, typically situated near the point-of-contact, assisting the operator/driver to guide the heads toward the point of interest. The operator can control the horizontal and vertical direction of the heads, while the alpine miners can move back and forth and side to side. The movement of the cutting heads is controlled by hydraulic

Reproduced with permission of the copyright owner. Further reproduction prohibited without permission.

pressure lines. The metal heads grind, crush and pulverize the native materials while an externally mounted hopper captures the loose material generated during the initial grinding operation. The loose material is then transferred away from the heading (i.e. face of the alcove or drift) with a conveyor belt that is externally attached to the alpine miner. The loose native material is now referred to as muck and is either transferred out of the immediate location (and hoisted out of the underground environment) or left in piles to be removed at a later time by a piece of equipment referred to as a mucker.

Once the muck is removed from the heading, the newly exposed underground surfaces need to be supported to prevent/minimize possible collapse. The first part to support the new surfaces is rock bolting. Rock bolting used various length (3 - 10 feet) metal bolts which are drilled into the underground surfaces. A flat 1-inch thick metal end-plate (8 inches by 8 inches) is attached to the end of the of rock bolt that have been drilled into the surface, which is tightened into the surface. A series of installed rock bolts within a given surface section results in compression forces due to the inward pressures of the end plate in equilibrium with the downward forces of the surrounding earth. These compression forces (in equilibrium) create a thick wall that surrounds the underground drift. The top of the drift (referred to as the back) is typically arched, thereby having the capability to evenly distribute externally compressive forces. The arched surface along with the rock bolts, provide the strength necessary to support the underground facility from collapse or cave-ins.

Large gauge metal wire mesh is next applied to the surfaces via connection to the rock bolt end plates on the surface of the ribs and back. This helps prevent loose native material from falling and causing a serious injury to workers in the area.

Reproduced with permission of the copyright owner. Further reproduction prohibited without permission.

The final step is covering the newly exposed underground surfaces and mesh with a cementacious material, fiber-crete. This material contains earthen soil products, cement and small metal fibers. It comes pre-packaged in 90-pound bags. The application process involves the addition of water in a mixer, and then pressure spraying the mix onto the surfaces. Drying takes about 24 hours. This mining process is continued for the duration of the underground drift/alcove construction.

The .05 drift, the location for sampling in this project, completed continuous mining activities one month prior to sampling. Therefore, determining fiber-crete's influence for radon emanation, with and without fiber-crete, could be observed without interfering with the underground construction schedule. Figure 2.5 shows the .05 drift, illustrating fiber creted and native material ribs.

This underground facility complies with the ventilation requirements specified in 29 CFR 1926.800, "Underground Construction." These requirements state that during construction operation phases in an underground environment, the ventilation must supply 200 cubic feet per minute (CFM) of fresh air per person, plus 2000 CFM of fresh air per welding operation and 100 CFM of fresh air per break horse power (BHP) of diesel-powered equipment. Currently the U1a Complex supplies approximately 65,000 CFM of fresh air during the hours of 0700 to 0300 (i.e. 20 hours per day), Monday through Friday morning. Ventilation is usually reduced to minimal flow from Friday morning to Monday morning. During extended work periods (i.e. overtime) the ventilation system is turned on to full capacity (65,000 CFM).

Reproduced with permission of the copyright owner. Further reproduction prohibited without permission.

2.4 Fiber Crete

The fiber crete used in the U1a Complex is called concrete mix #1101. It is manufactured by the QUIKRETE Companies, with its headquarters in Atlanta, Georgia. The material safety data sheet specifies that the major constituents are silica sand, portland cement, gypsum, lime, fly ash, calcium aluminate cement, and pulverized limestone. The specific proportions used to make this product are proprietary information. It also contains 1-inch carbon steel wire, which is used as a strengthening agent. The fibers make up approximately 1.0% (by weight) of the dry weight fiber crete. The remaining percentages are 72% aggregate and 27% 200-mesh size material. The basic materials are quarried in the Salt Lake City, Utah, area.

Application requires mixing the dry fiber crete with enough water to form a slurry. This mixture is then sprayed onto the underground surfaces at the required thickness. U1a surfaces are coated twice; each with a thickness of three inches. Samples are cored at approximately 12 hours after application. The core sample is allowed to cure for a minimum of 28 days, followed by a compressive strength test per the American Society for Testing and Materials test method C 39-96, "Standard Test Method for Compressive Strength of Cylindrical Concrete Specimens." The basic test method consists of applying a compressive axial load to the core sample at a specific rate and within a prescibed range until failure occurs. The compressive strength is calculated by dividing the maximum load attained by the cross-sectional area of the core sample (ASTM, 1994). The compressive strength must meet or exceed 6000 psi.

Reproduced with permission of the copyright owner. Further reproduction prohibited without permission.

2.5 Sampling and Analytical Strategy

Sampling and analysis was conducted in three phases: 1) initial analysis of soils and building materials (fiber crete) with gamma spectroscopy, 2) emanation of radon gas from soils and fiber crete using alpha scintillation, and 3) collection of radon gas and radon daughters released via exhalation with analysis by gamma spectroscopy. The overall sampling and analytical procedure is outlined in the following sections.

2.5.1 Collection of Soils and Fiber Crete and Analysis by γ - Spectroscopy

Collection of in-situ materials was prepared and analyzed by gamma spectroscopy. Native material was collected directly from the underground facility ribs, in the 05 drift of the U1a Complex. This involved collecting a batch supply of native material with a shovel and placing the material in a large, heavy-duty plastic bag. Fiber crete was collected by direct transfer (i.e pouring) from 90-lb product packages to the same type of heavy-duty plastic bag. The batch samples were brought to the UNLV Health Physics laboratory and prepared for gamma spectroscopy with an initial oven drying at 100 °C for one week. This was followed by measuring a specific volume of material and transferring the material in high density polyethylene (HDPE) bottles. Initially, seven bottles of native material were prepared: three were measured to 250 ml and four were measured to 500 ml. Eight fiber crete samples were prepared: four at 250 ml and four at 500 ml. This would allow gamma spectroscopy results to show, not only a comparison of native material and fiber crete radon activities, but also a comparison between the two types of geometries.

In addition to dried fiber crete, a batch supply of fiber crete was mixed with industrial water (collected from the U1a Complex industrial water lines) and placed in

Reproduced with permission of the copyright owner. Further reproduction prohibited without permission.

500 ml HDPE bottles where the material cured for one week. Six 500 ml samples were prepared. Pre and post weighing was conducted on all bottles to determine to water loss due to evaporation. To account for any activity that might be attributed to the industrial water, a separate gamma spectroscopy of the water was conducted.

All sample bottles were tightly sealed for a minimum of 28 days. This allowed for secular equilibrium between ^{222}Rn and its parent, ^{226}Ra, and ^{222}Rn progeny and ^{222}Rn to be achieved. The HDPE bottles had approximate dimensions of 6.4 cm radius and 18 cm high (including the bottle's neck). A volumetric experiment indicated a total water capacity of 545 ml. Samples were either placed in the HDPE bottles and filled to a pre-marked level, or first measured with a graduated beaker and then placed in the HDPE bottle. The "Discussion" section elaborates further on these two measuring techniques.

The instrument used to detect and quantify gamma energies was a Canberra gamma-ray spectroscopy system, with a high purity germanium (HPGE) detector. Peaks for numerous radionuclides associated with the ^{238}U decay chain were quantified, yielding an activity concentration per unit soil (pCi kg^{-1} or Bq kg^{-1}). From this activity concentration, the radon concentration was calculated, based on radon's half-life and subsequent equilibrium with these radionuclide's measured activity. Units were expressed in Bq g^{-1}. This activity represents the maximum radon available in the soil, disregarding the emanation and exhalation factors.

2.5.2 Collection of Soils and Fiber Crete with Analysis by Scintillation

Scintillation counting, for the detection of radon gas emanating from soils and fiber crete was accomplished with a Lucas cell. The Lucas cell is a device with a known

Reproduced with permission of the copyright owner. Further reproduction prohibited without permission.

volume coated with ZnS(Ag) connected to a photomultiplier tube. This cell is typically constructed of glass or metal and can be spherical, cylindrical or conical. Volumes can range from 0.1 to 3 liters. The inside is spray coated with a ZnS(Ag) suspension in ethylene dichloride (Budnitz 1974) to a thickness of 20 mg cm^{-2} of phosphor. There is a quartz window in which scintillations are viewed by a connected photomultiplier tube (PMT). The inner surface of the quartz window is coated with a transparent layer of tin oxide designed to eliminate any induced negative charges that would develop from the photocathode during contact with the PMT face. Without this coating, radon progeny would deposit on the window, resulting in detection variations up to 15% (NCRP 1988).

Air samples are drawn into the cell by either a pump or by evacuation. A micro stopcock is used for filling and evacuating the cell. All samples are filtered prior to reaching the lucas cell chamber by a dryer filter with $CaCl_2$ that removed water vapor, radon daughters and aerosols, so that only the parent radon gas is admitted into the cell for scintillation (Shimo et al, 1987). Once in the chamber cell, the radon gas is allowed to decay and reach equilibrium with its progeny. Because ^{214}Pb has the largest half-life (approximately 27 minutes) of the immediate radon progeny equilibrium, 3.5 hours, or seven half-lives, would be considered as appropriate time to wait prior to counting. Thus, the alpha detection by the ZnS(Ag) phosphor is a measure of radon, ^{218}Po, and ^{214}Po. ^{222}Rn, ^{218}Po, and ^{214}Po have decay energies of 5.49, 6.00, and 7.68 MeV, respectively.

While interferences from ^{220}Rn (thoron) and ^{219}Rn (actinon) are possible (both are alpha-emitters), their interferences are considered small due to their short half-lives of 55 seconds and 4 seconds, respectively (Budnitz, 1974). The lower limit of detection (LLD)

Reproduced with permission of the copyright owner. Further reproduction prohibited without permission.

of typical Lucas cell analyses is 0.1 pCi (4 mBq) for a 60-minute count at a 95% confidence level (NCRP 1988).

Analysis with the Lucas cell involved connecting the 100-ml cell cavity to a 500-ml HDPE bottle that contained the source material by plastic tubing. . The plastic tubing was pinched closed with an acetyl hose clamp. The HDPE bottle, containing the native material or cured fiber crete, was sealed for 39 days (over 9 ½-lives), therefore, allowing the radon to attain equilibrium with its progeny. A #10 rubber stopper (with a single hole) was placed on the HPDE bottle with teflon tape to insure a tight seal and allow attachment of the plastic tubing.

The HDPE bottle was connected to a series of capillary tubes (outside diameter of 7.5 mm and an inside diameter of 1.90 mm) which serves the purpose of connecting the Lucas cell, HDPE bottle and pressure gauge together. Directly above the bottle clamp was a moisture trap made with anhydrous calcium sulfate.

Prior to releasing the gases emanating from the source material to the Lucas cell, the lucas cell was evacuated via the laboratory pump. At this point, only the Lucas cell valve was open. Once the vacuum pressure was recorded, the vacuum was closed and the valve to the moisture trap was opened (the clamp to the HDPE bottle remained closed). This would result in a pressure change as the volume changed due to the addition of the moisture trap and part of the plastic tubing to the HDPE bottle. Using Boyle's Law, the additional volume could be calculated by:

$$P_1V_1 = P_2V_2 \qquad (2.1)$$

where:

Reproduced with permission of the copyright owner. Further reproduction prohibited without permission.

V_1 = Volume of the Lucas cell (100 cm^3) and capillary tubing to moisture trap valve,

P_1 = Recorded pressure of V_1.

V_2 = Volume associated with V_1 plus the added volume of the moisture trap and portion of the plastic tubing to the hose clamp near the HDPE bottle clamp,

P_2 = Pressure associated with V_2.

At this point, the volume between the two valves can be calculated simply by subtracting V_1 from V_2.

Next the bottle clamp was opened which allowed the lucas cell to be filled with the emanating gases from the source material. The system pressure was again recorded and Boyle's Law was applied to calculate the sample bottle's head space and source material void spaces (including a small portion of the plastic tubing connecting the bottle to the clamp). The system valves were left open for approximately two minutes, allowing the emanating gases to equilibrate throughout the system, thereby giving the Lucas cell a representative sample of the emanating gases.

After the Lucas cell was filled with the emanated gases it was left to equilibrate (between radon and its progeny) for approximately four hours before being placed in a sealed container that was attached to the PMT (Manufacturer: Rocky Mountain Scientific Glass Blowing Company, Denver, Colorado). Each Lucas cell was pre-counted for background activity and pre-calibrated, accounting for cpm dpm^{-1}, based on the cell's surface area coated with the zinc sulfide scintillation material and the additional activity due to radon's progeny. Therefore, calculations of the activity, attributed to solely to

Reproduced with permission of the copyright owner. Further reproduction prohibited without permission.

radon gas, could be made. Counting was conducted by a Ludlum scaler instrument, model 1000, operating at 900 volts. This instrument has an adjustable time counter (in minutes) that automatically shuts down once the specified time is reached, while retaining the actual counts. Figures 2.10 and 2.11 show the Lucas Cell, PMT and Ludlum Scaler . After the counting time was completed and the total counts was recorded, the count rate was calculated by dividing net counts by the counting time and the specific Lucas cell's efficiency factor. This number was the number of disintegrations per minute (dpm) associated with the amount of gas in the Lucas cell exclusively and not the entire emanated gas generated from the source material. To calculate the activity of the entire gas emanated, the calculated dpm was multiplied by the ratio of the entire system volume (Lucas cell, capillary tubing, moisture filter, plastic tubing, bottle head space and material void space) over the Lucas cell volume (100 cm^3). This resulted in a radon activity attributed to all of the emanating gas and is expressed as activity per sample. By dividing this number by the sample weight, and converting the activity into Becqurels (dividing activity by 60 seconds), the sample's activity concentration of ^{222}Rn was then expressed in Bq g^{-1}. The emanation coefficient was then calculated by dividing this activity concentration by the activity concentration obtained from the initial gamma spec activity for each unique sample.

Reproduced with permission of the copyright owner. Further reproduction prohibited without permission.

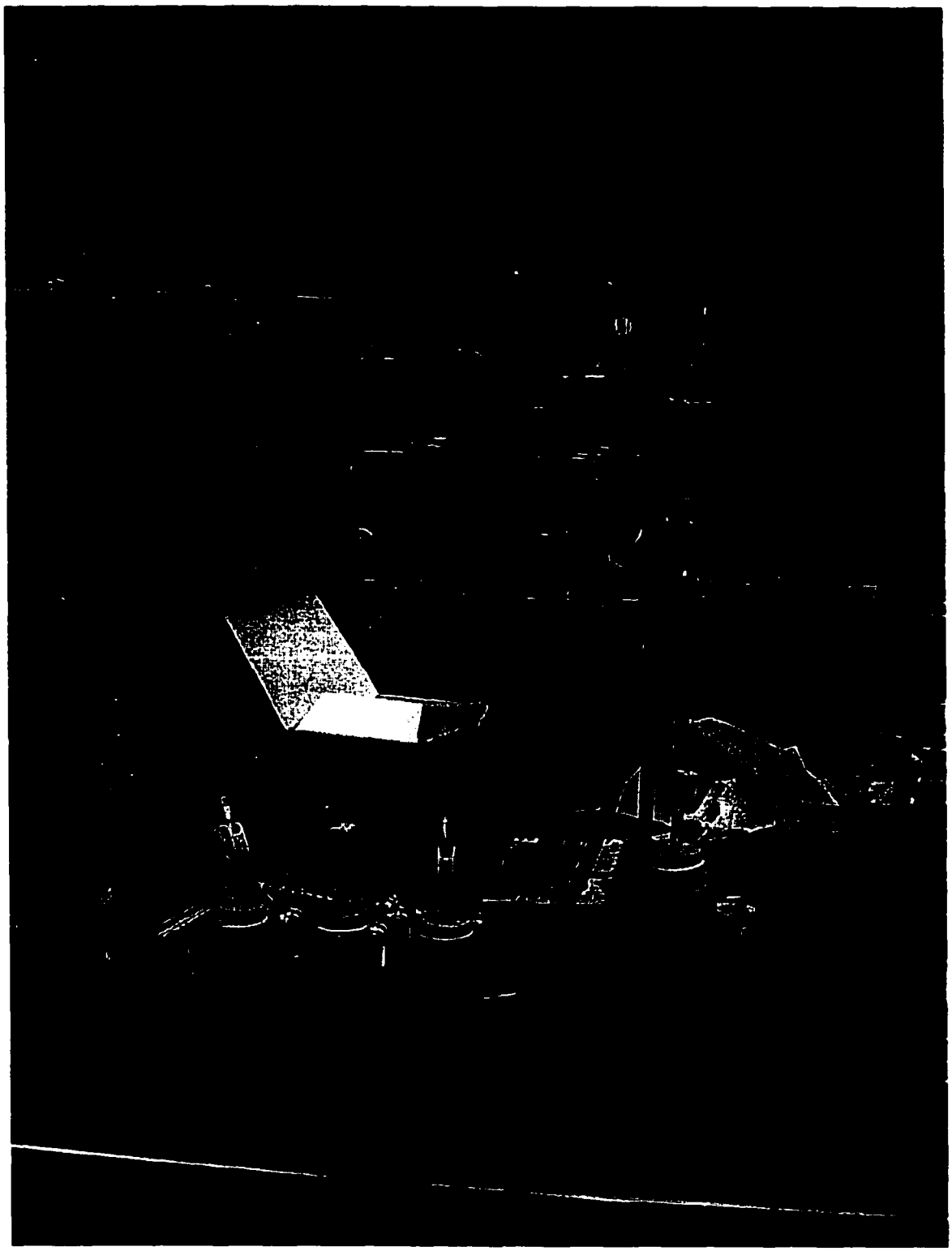

Figure 2.2 500- ml HDPE Bottle Connected to Lucas Cell

Reproduced with permission of the copyright owner. Further reproduction prohibited without permission.

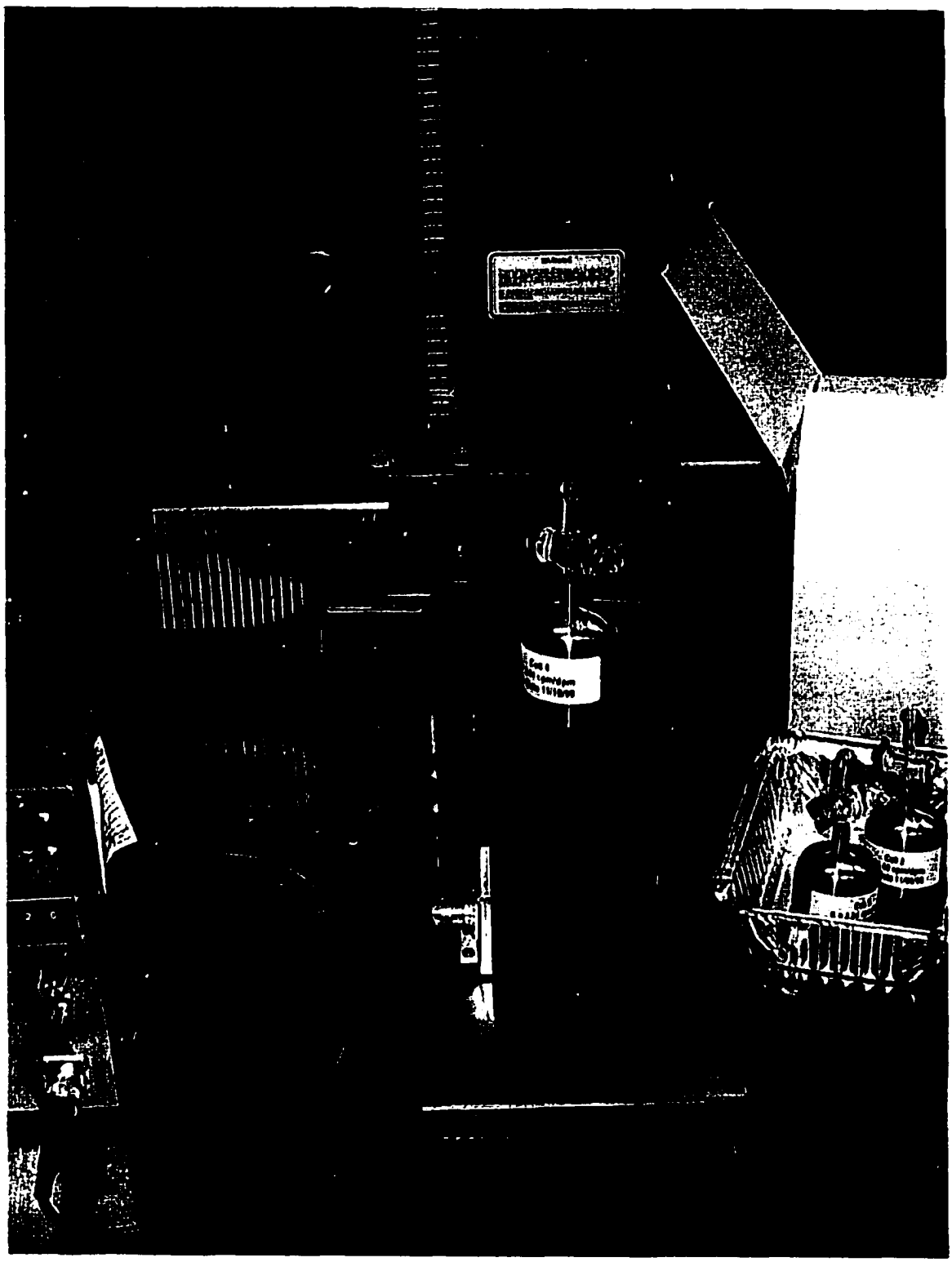

Figure 2.3 Lucas Cell Placed on PMT with Scalar

Reproduced with permission of the copyright owner. Further reproduction prohibited without permission.

2.6 Radon Exhalation Analysis with Charcoal Canisters

The first person to verify that charcoal was a viable collection media for radon was the renowned English scientist, Ernest Rutherford (NCRP 1988). Today charcoal canisters are used to quantify radon gas for indoor air studies in office buildings and homes. While charcoal canisters are used primarily to asses indoor air quality for office and residential environments, Countess (1976) suggested that radon flux measurements can be made by passive diffusion canisters.

2.6.1 Measurement of Diffusion Barrier Charcoal Canisters

Radon has a strong affinity for activated charcoal. The term, "activated charcoal" refers to a pre-burnt material, typically coconut that is subjected to high temperature steam (1000°C), which increases the charcoal's absorption properties (National Safety Council 1988). After radon gas enters the adsorption sites, radon decays to its progeny. Within three hours the progeny are in equilibrium with the parent. Counting is determined by gamma spectroscopy, based on the gamma emission peaks of ^{214}Pb (295 keV and 352 keV) and ^{214}Bi (609 keV).

For this study, charcoal canisters were placed on the underground ribs. These canisters were placed on the ribs at locations where fiber crete was applied or not applied (i.e. native material surfaces). The initial sampling protocol was designed for collection times ranging from three to ten days.

After collection, the canisters were opened and the charcoal/collection media was analyzed by gamma spectroscopy for radon daughters (^{214}Pb and ^{214}Bi). The results were used to calculate the amount of radon exhalation activity (Bqs l^{-1} sec^{-1}), thus representing

Reproduced with permission of the copyright owner. Further reproduction prohibited without permission.

the amount of radon exposure within the underground location that is attributed to exhalation for the rib surfaces. The difference in exhalation rates for fiber creted and non-applied surfaces were then compared to each other to determine the effects of airborne radon gas within this specific environment from the application of building materials. Results were recorded and a comparison between sampling times and the two surface materials were observed.

All canisters were supplied by the U.S. EPA, located in Las, Vegas, Nevada, on the UNLV campus. Each canister had its own EPA identifying control number. These numbers were assigned one of the unique collection numbers described in section 2.6.2, "InSitu Sampling." Therefore the analysis of each canister could be identified to its unique location, sample material and collection time.

Modern charcoal canisters, such as the EPA open-face canister, consists of an 8-ounce metal can (10-cm diameter by 2.9-cm deep), with 70 ± 1 g of 6 x 16 mesh activated charcoal. A metal screen is used to secure the charcoal bed, while allowing radon gas to come in contact with the active sites (Gray, Windham 1990). As a way to protect the charcoal bed from physical damage, a 1.25-mm thick polyethylene membrane with twenty 2.3-mm diameter holes is placed to retain the bed.

Aside from good adsorption properties, the activated charcoal must have a low radioactive content. Gamma emitters, except for natural ^{40}K, must be less than 7.4 mBq g^{-1} (Gray and Windham, 1990).

At the end of each collection period, the canisters were closed, taped and the exact time recorded (recorded times include beginning and ending times). Analysis was not conducted earlier than three hours after collection to ensure equilibrium with the radon,

Reproduced with permission of the copyright owner. Further reproduction prohibited without permission.

while also no later than four days, as desorption may occur. Counting was conducted for 10-minuite periods using an NaI detector. The count time and detector efficiency (conducted daily) was recorded. This was followed by the radon activity calculation using the following equation:

$$Rn = (\text{Net CPM})/(T_s \times E \times CF \times DF) \quad (2.2)$$

where:

Rn = radon concentration in pCi l^{-1},

Net CPM = (gross CPM for the canister) - (background CPM for the detector),

T_s = canister exposure time (minutes),

E = detector efficiency (CPM pCi^{-1}),

CF = calibration factor (liters $minute^{-1}$),

DF = decay factor (from midpoint of exposure period to start of counting), and

Of the above-listed variables, CF and DF need further explanations.

CF is the air influx (L min^{-1})and can be calculated by rearranging the above equation. The EPA has collected empirical data and has listed CFs based upon percent humidity (Gray and Windham, 1990).

The DF is used to correct for radiological decay between exposure and counting times. It is calculated from the midpoint of exposure to the start of analytical counting using the formula:

$$DF = e^{(-0.693t/T_{1/2})} \quad (2.3)$$

where:

t = time from midpoint of exposure to the start of counting, and

Reproduced with permission of the copyright owner. Further reproduction prohibited without permission.

$T_{1/2}$ = half-life of ^{222}Rn (3.82 days).

The result is the airborne concentration of radon gas in the sampled environment.

2.6.2 In-Situ Sampling

In-situ sampling for native material radon exhalation was conducted in a pit within the .05 drift, approximately five feet off the fiber creted rib while radon exhalation for the fiber creted surfaces was conducted simultaneously with canisters placed directly on the rib. While the geology of the two surfaces used for in-situ sampling are considered to be the same, gamma-spectroscopy of the native materials that comprise the two locations, was conducted and compared to each other. The results were used to verify that the native materials for both locations had similar activities. Therefore, exhalation values for both locations could be compared to each other, with the assumption that different exhalation values can be attributed to the different surface materials.

The strategy for data collection required coordination with the U1a Complex management, as sampling could not interfere with the ongoing underground activities. Charcoal canisters were placed within close proximity to the rib surfaces allowing for diffusion of radon gas within the individual canisters from the exhalating surfaces. Initially, it was thought that creating a tight seal between the canister edge and exhalating surfaces would inhibit radon migration into the canisters due to the creation of a pressure build-up within the canister, thus allowing for radon to migrate around the canister and escape into the drift atmosphere. Seven groups of three canisters were set up within the .05 drift for both surface types. Collection time periods were three, seven and ten days, with seven canisters, one from each of the seven groups, to be removed from the sampled surface during each of time periods.

Reproduced with permission of the copyright owner. Further reproduction prohibited without permission.

The charcoal canisters were secured to the surfaces with 6-foot length angle iron (90°) with duct tape used to secure the canisters in place. The canisters that collected radon from the native material surfaces were placed in two rows, one directly above the other with the upper row consisting of four 3-canister groupings, and the second row having three groups (also with three canisters per group). Canisters that collected radon from the fiber crete surface were placed in two rows, next to each other. The reason for the two different configurations was due to the uneven surfaces, thus influencing the ability of the installed angle iron to provide adequate gas collection distances from their respective surfaces. The sampling configuration used for canister placement, along with the numbering system, is represented below.

11 12 13 21 22 23 31 32 33 41 42 43

51 52 53 61 62 63 71 72 73

Sampling for radon gas exhalated from both the fiber crete and native material surfaces was conducted simultaneously, thereby reducing the total experiment time since no wait period for the fiber crete to cure (28 day cure time) was necessary. This was crucial, as access to the complex for conducting this experiment was limited due to the ongoing underground activities. Another advantage to simultaneous sampling is that both surfaces were subject to the same influences. Therefore a change in ventilation, humidity, or pressure would not have to be duplicated (an impossible task) in order to ensure the environmental conditions were not attributing to any differences in activities between the two surface exhalations.

Reproduced with permission of the copyright owner. Further reproduction prohibited without permission.

After samples were removed from their collection locations, they were sent to the EPA Laboratory at UNLV. Because of ^{222}Rn's 3.82-day half-life, all samples had to be analyzed within eight hours after the sample collection period was completed.

Ventilation in the .05 drift was designed to be maintained at a constant rate. Typically, the ventilation rate in the .05 drift was 9000 CFM. Temperature, pressure and relative humidity were continuously monitored. While temperature is not expected to be an influence on radon transport through the underground materials, humidity and pressure have been shown to affect exhalation values. Therefore, changes in pressure and relative humidity (i.e. moisture) need to be closely monitored.

Reproduced with permission of the copyright owner. Further reproduction prohibited without permission.

CHAPTER III

RESUTLTS

3.1 Analysis of Native Materials and Fiber Crete

Two sets of native material samples were analyzed due to a change in the In-Situ sampling location. The location change occurred after the initial gamma spectroscopy for native materials was conducted. The two sampling sets are referred to as "First Round" and "In-Situ" sampling locations. The "First Round" samples were taken in the same area where the fiber crete exhalation occurred. Gamma spectroscopy results for the two sampling locations were compared to each other to determine if a significant difference in activities existed. Similar activities would support the assumption of similar lithogies and soil-types, and therefore, support a direct comparison between the exhalation rates for the fiber crete and native material surfaces, even though their locations differed slightly.

Tables 3.1 - 3.5 display the physical data for the First Round and In-Situ native materials, dry and cured fiber crete, and the U1a Complex industrial water (used to create the cured fiber crete). The information included dates of preparation and analysis, counting times, samples volumes, masses and densities.

Reproduced with permission of the copyright owner. Further reproduction prohibited without permission.

Reproduced with permission of the copyright owner. Further reproduction prohibited without permission.

Table 3.1: Physical Data for Gamma Spectroscopy, Native Material (First-Round Sampling)

Sample #	Date Prepared	Date Analyzed	Counting Time (seconds)	Volume (ml)	Mass (grams)	Density (g cm^{-3})
RB0121S1	1/21/00	3/7/00	91,065	250	319.1	1.276
RB0121S2	1/22/00	3/25/00	65,054	250	327.3	1.309
RB0121S3	1/21/00	3/8/00	17,860	250	328.6	1.314
RB0204S1	2/4/00	2/23/00	20,352	500	663.5	1.327
RB0204S2	2/4/00	3/6/00	139,353	500	665.7	1.331
RB0204S3	2/4/00	2/29/00	68,915	500	652.3	1.305
RB0205S1	2/5/00	3/4/00	59,132	500	672.4	1.345

Table 3.2: Physical Data for Gamma Spectroscopy, Native Material of In-Situ Sampling Location

Sample #	Date Prepared	Date Analyzed	Counting Time (seconds)	Volume (ml)	Mass (grams)	Density (g cm^{-3})
RB0407S1	4/7/00	5/2/00	300,000	500	612.9	1.22
RB0407S2	4/7/00	7/7/00	61,295	500	609.5	1.22
RB0407S3	4/7/00	5/4/00	93,307	500	598.7	1.20
RB0407S4	4/7/00	5/5/00	53,294	500	621.0	1.24
RB0407S5	4/7/00	5/8/00	293,897	500	635.8	1.27
RB0407S6	4/7/00	5/9/00	52,745	500	657.0	1.31

Reproduced with permission of the copyright owner. Further reproduction prohibited without permission.

Table 3.3: Physical Data for Gamma Spectroscopy, Fiber Crete (Dry)

Sample #	Date Prepared	Date Analyzed	Counting Time (seconds)	Volume (ml)	Mass (grams)	Density (g cm^{-3})
RB0204F1	2/4/00	3/30/00	157,697	250	419.8	1.679
RB0204F2	2/4/00	3/8/00	83,295	250	455.4	1.822
RB0204F3	2/4/00	3/27/00	175,093	250	448.8	1.795
RB0204F4	2/4/00	3/28/00	98,877	250	449.0	1.796
RB0205F1	2/5/00	3/1/00	60,852	500	869.7	1.735
RB0205F2	2/5/00	3/3/00	105,842	500	865.7	1.731
RB0205F3	2/5/00	3/2/00	77,013	500	875.6	1.751
RB0205F4	2/5/00	3/4/00	25,769	500	869.4	1.739

Table 3.4: Physical Data for Gamma Spectroscopy, Cured Fiber Crete (Industrial Water Added)

Sample #	Date Prepared	Date Analyzed	Counting Time (seconds)	Volume (ml)	Mass (grams)	Density (g · cm^{-3})
RB0311C1	3/11/00	4/7/00	182,175	500	1025	2.050
RB0311C2	3/11/00	4/12/00	175,356	500	1037	2.074
RB0311C3	3/11/00	4/3/00	151,246	500	1046	2.092
RB0311C4	3/11/00	4/4/00	94,878	500	1071	2.142
RB0311C5	3/11/00	4/8/00	55,474	500	1035	2.069
RB0311C6	3/11/00	4/10/00	176,781	500	1035	2.069

Table 3.5: Physical Data for Gamma Spectroscopy, U1a Industrial Water

Sample #	Date Prepared	Date Analyzed	Counting Time (seconds)	Mass (grams)	Volume (liters)	Density (g cm^{-3})
RB031100-01W	3/11/00	3/20/00	235,2130	3268	3.3	0.990

Tables 3.6 - 3.10 present the activity concentrations of selected radionuclides from the five material types mentioned above. These radionuclides were ^{40}K, ^{210}Pb, ^{214}Pb, ^{214}Bi, ^{224}Ra, ^{228}Ac, ^{234}Ac, ^{234}Th, and ^{235}U. While ^{210}Pb, ^{214}Pb, and ^{214}Bi, and ^{234}Th are part of the ^{238}U-decay series, the other radionuclides, such as ^{40}K, may serve as a comparison with soils from other studies, thereby supporting or refuting this study's gamma spectroscopy results.

Tables 3.11 - 3.20 focused on the gamma spectroscopy data for ^{214}Pb and ^{214}Bi, and the calculated activity of ^{222}Rn, including the statistical data for these radionuclides. The statistics include high, low and average activities, plus the standard deviations of the average activity concentrations.

Tables 3.17 and 3.18 display data for uncorrected fiber crete activities, while Tables 3.19 and 3.20 show the data for corrected fiber crete activities. The terms "corrected" and "uncorrected" refer to calculations of the gamma spectroscopy measurement data that consider the Ula industrial water used in the fiber crete mixing process. This was necessary as the activity concentration had to be equated to the mass of the fiber crete and not to the collective masses of the fiber crete and water. Otherwise the measured activity concentrations would be underestimated. Table 3.21 is a comparative summary of the physical characteristics of pre and post cured fiber crete samples. This table specifies the amount of water left in each sample, which, in turn, determines the corrected amount of fiber crete that contributes to the measured activity from gamma spectroscopy.

Reproduced with permission of the copyright owner. Further reproduction prohibited without permission.

Reproduced with permission of the copyright owner. Further reproduction prohibited without permission.

Table 3.6: Selected Radionuclides from Gamma Spectroscopy of Native Materials (First-Round Sampling): (Bq g^{-1})

Nuclide	RB0204S 1	Uncertainty (±)	RB0204S 2	Uncertainty (±)	RB0204S3	Uncertainty (±)	RB0205S1	Uncertainty (±)
K-40	0.767	0.0368	0.761	0.0297	0.760	0.0302	0.773	0.0309
Tl-208	0.0203	0.00103	0.0206	0.00066	0.0204	0.00076	0.0205	0.00073
Pb-210	ND	NA	0.0302	0.00647	ND	NA	0.0336	0.00923
Bi-214	0.0380	0.00180	0.0399	0.00106	0.0398	0.00125	0.0421	0.00138
Pb-214	0.0374	0.00183	0.0378	0.00137	0.0387	0.00150	0.0403	0.00155
Ra-224	0.0416	0.00919	0.0341	0.00684	0.0387	0.00759	0.0321	0.00754
Ac-228	0.0607	0.0253	0.0608	0.00099	0.0622	0.00159	0.0591	0.00130
Th-234	0.0444	0.00747	0.0500	0.00504	0.0565	0.00639	0.0577	0.00630
U-235	0.0049	0.00068	0.0045	0.00042	0.0044	0.00052	0.0042	0.00052

Table 3.6 (Continued): Selected Radionuclides from Gamma Spectroscopy of Native Materials (First-Round Sampling): (Bq g^{-1})

Nuclide	RB0121S1	Uncertainty (±)	RB0121S2	Uncertainty (±)	RB0121S3	Uncertainty (±)
K-40	0.770	0.0300	0.805	0.0317	0.781	0.0337
Tl-208	0.0202	0.00073	0.0209	0.00076	0.0192	0.00096
Pb-210	0.0425	0.00715	0.0333	0.00864	0.0323	0.0172
Bi-214	0.0417	0.00127	0.0421	0.00132	0.0403	0.00191
Pb-214	0.0375	0.00123	0.0390	0.00138	0.0376	0.00183
Ra-224	0.0326	0.00574	0.0365	0.00631	0.0314	0.00819
Ac-228	0.0617	0.00115	0.0634	0.00128	0.0595	0.00206
Th-234	0.0488	0.00518	0.0526	0.00568	0.0345	0.00906
U-235	0.0049	0.00047	0.0050	0.00052	0.0063	0.00091

ND - non detect, energy peaks associated with a specific radionulcide were not detectable
NA - not applicable due to non-detectable energy peaks
Samples RB0204S1,S2,S3 and RB0205S3 = 500 ml volume
Samples RB0121S1 and S3 = 250 ml volume

Reproduced with permission of the copyright owner. Further reproduction prohibited without permission.

Table 3.7: Selected Radionuclides from Gamma Spectroscopy of Native Materials at In-Situ Sampling Location: (Bq g^{-1})

Nuclide	RB0407S1	Uncertainty (±)	RB0407S2	Uncertainty (±)	RB0407S3	Uncertainty (±)
K-40	0.806	0.0312	0.813	0.0320	0.828	0.0326
Tl-208	0.0217	0.00060	0.0205	0.00074	0.0215	0.00074
Pb-210	0.0257	0.00638	0.0296	0.00972	0.0542	0.0105
Bi-214	0.0396	0.00098	0.0395	0.00125	0.0402	0.00121
Pb-214	0.0383	0.00138	0.333	0.00139	0.0388	0.00152
Ra-224	0.0392	0.00701	0.0401	0.00664	0.0371	0.00743
Ac-228	0.0597	0.00084	0.0592	0.00118	0.0620	0.00119
Th-234	0.0409	0.00373	0.0553	0.00650	0.0593	0.00589
U-235	0.0038	0.00032	0.0586	0.00056	0.0047	0.00048

Table 3.7 (Continued): Selected Radionuclides from Gamma Spectroscopy of Native Materials at In-Situ Sampling Location: (Bq g^{-1})

Nuclide	RB0407S4	Uncertainty (±)	RB0407S5	Uncertainty (±)	RB0407S6	Uncertainty (±)
K-40	0.791	0.0032	0.764	0.0296	0.7660	0.0308
Tl-208	0.0194	0.0007	0.0213	0.0006	0.0195	0.0008
Pb-210	0.0387	0.0099	0.0300	0.0061	0.0167	0.0088
Bi-214	0.0393	0.0014	0.0384	0.0009	0.0388	0.0013
Pb-214	0.0378	0.0016	0.0369	0.0013	0.0362	0.0015
Ra-224	0.0291	0.0073	0.0333	0.0065	0.0287	0.0071
Ac-228	0.0576	0.0014	0.0565	0.0008	0.0578	0.0014
Th-234	0.0445	0.0072	0.0415	0.0037	0.0424	0.0062
U-235	0.0055	0.0006	0.0047	0.0004	0.0043	0.0005

All samples were 500 ml volume

Reproduced with permission of the copyright owner. Further reproduction prohibited without permission.

Table 3.8: Selected Radionuclides from Gamma Spectroscopy of Fiber Crete: (Bq g^{-1})

Nuclide	RB0205F1	Uncertainty (±)	RB0205F2	Uncertainty (±)	RB0205F3	Uncertainty (±)	RB0205F4	Uncertainty (±)
K-40	0.525	0.0218	0.549	0.0216	0.551	0.0218	0.537	0.0226
Tl-208	0.0061	0.0003	0.0059	0.0003	0.0060	0.0003	0.0064	0.0005
Pb-210	0.0059	0.0036	0.0141	0.0050	0.0011	0.0035	0.0006	0.0084
Bi-214	0.0173	0.0007	0.0175	0.0006	0.0162	0.0006	0.0182	0.0009
Pb-214	0.0155	0.0007	0.0154	0.0006	0.0146	0.0007	0.0169	0.0010
Ra-224	0.0100	0.0032	0.0103	0.0029	0.0103	0.0030	0.0083	0.0042
Ac-228	0.0184	0.0006	0.0190	0.0005	0.0183	0.0006	0.0196	0.0010
Th-234	0.0123	0.0029	0.0148	0.0031	0.0082	0.0032	0.0113	0.0054
U-235	0.0022	0.0003	0.0018	0.0003	0.0018	0.0003	0.0020	0.0005

Table 3.8 (Continued): Selected Radionuclides from Gamma Spectroscopy of Fiber Crete: (Bq g^{-1})

Nuclide	RB0204F1	Uncertainty (±)	RB0204F2	Uncertainty (±)	RB0204F3	Uncertainty (±)	RB0204F4	Uncertainty (±)
K-40	0.529	0.0204	0.509	0.0200	0.531	0.0204	0.522	0.0203
Tl-208	0.0064	0.0003	0.0071	0.0003	0.0065	0.0003	0.0061	0.0003
Pb-210	0.0083	0.0036	0.0079	0.0052	0.0048	0.0035	0.0049	0.0031
Bi-214	0.0176	0.0006	0.0182	0.0007	0.0190	0.0006	0.0179	0.0007
Pb-214	0.0159	0.0006	0.0161	0.0006	0.0166	0.0006	0.0154	0.0006
Ra-224	0.0106	0.0024	0.0102	0.0026	0.0118	0.0025	0.0101	0.0025
Ac-228	0.0200	0.0005	0.0211	0.0006	0.0203	0.0005	0.0200	0.0006
Th-234	0.0119	0.0025	0.0169	0.0030	0.0109	0.0024	0.0134	0.0027
U-235	0.0023	0.0003	0.0020	0.0003	0.0021	0.0002	0.0019	0.0003

RB0205F3, Th-234; one gamma peak (63.29 keV) had a measured activity < calculated uncertainty (52.4% Confidence at 1σ)

RB0205F3 and RB0205F4: activity for Pb-210 indicates activity < uncertainty value

RB0205F3, Th-234; one gamma peak (63.29 keV) had a measured activity < calculated uncertainty (52.4% Confidence at 1 σ)

RB0205F3 negative activity for Pb-210 indicates activity < background, while confidence = 99.8%

Reproduced with permission of the copyright owner. Further reproduction prohibited without permission.

Table 3.9: Selected Radionuclides from Gamma Spectroscopy of Cured Fiber Crete with Industrial Water: (Bq g^{-1})

Nuclide	RB0311-01C	Uncertainty (±)	RB0311-02C	Uncertainty (±)	RB0311-03C	Uncertainty (±)
K-40	0.441	0.0172	0.433	0.0169	0.421	0.0164
Tl-208	0.0053	0.0002	0.0054	0.0002	0.0051	0.0002
Pb-210	0.0002	0.0030	0.0037	0.0030	0.0075	0.0031
Bi-214	0.0121	0.0004	0.0004	0.0004	0.0123	0.0004
Pb-214	0.0109	0.0005	0.0005	0.0005	0.0112	0.0005
Ra-224	0.0103	0.0022	0.0022	0.0022	0.0092	0.0022
Ac-228	0.0166	0.0004	0.0004	0.0004	0.0154	0.0004
Th-234	0.0094	0.0021	0.0019	0.0019	0.0087	0.0021
U-235	0.0016	0.0002	0.0002	0.0002	0.0016	0.0002

Table 3.9 (Continued): Selected Radionuclides from Gamma Spectroscopy of Cured Fiber Crete with Industrial Water: (Bq g^{-1})

Nuclide	RB0311-04C	Uncertainty (±)	RB0311-05C	Uncertainty (±)	RB0311-06C	Uncertainty (±)
K-40	0.419	0.0165	0.428	0.0167	0.428	0.0167
Tl-208	0.0054	0.0003	0.0057	0.0002	0.0054	0.0002
Pb-210	0.0056	0.0035	0.0068	0.0034	0.0017	0.0030
Bi-214	0.0119	0.0005	0.0128	0.0004	0.0122	0.0004
Pb-214	0.0109	0.0005	0.0114	0.0005	0.0110	0.0005
Ra-224	0.0090	0.0023	0.0077	0.0021	0.0096	0.0021
Ac-228	0.0156	0.0005	0.0160	0.0004	0.0160	0.0004
Th-234	0.0115	0.0024	0.0124	0.0021	0.0097	0.0022
U-235	0.0015	0.0002	0.0015	0.0002	0.0019	0.0002

RB0311-01C, 02C: activity for Pb-210 indicates activity < uncertainty value

Reproduced with permission of the copyright owner. Further reproduction prohibited without permission.

Table 3.10 : Selected Radionuclides from Gamma Spectroscopy

Industrial Water: (Bq g^{-1})

Nuclide	RB0311-01W	Uncertainty (±)
K-40	0.0005	0.00025
Tl-208	0.0002	0.00007
Pb-210	0.0002	0.00089
Bi-214	0.00002	0.00003
Pb-214	0.0001	0.00005
Ra-224	ND	NA
Ac-228	0.00004	0.00005
Th-234	0.0004	0.00039
U-235	0.00004	0.00010

ND - non detect, energy peaks associated with specific radionulcide were not detectable
NA - not applicable due to non-detectable energy peaks
Activity for Pb-210 and U-235 indicates activity < uncertainty value

Table 3.11: The Calculated Activity of Radon From its Progeny Gamma Spectroscopy of Native Material Samples (First-Round Sampling)

Sample #	Pb-214 (Bq g^{-1})	Bi-214 (Bq g^{-1})	Ratio (Pb-214/Bi-214)	Rn-222 (Bq g^{-1})
RB0204S1	0.0374	0.0380	0.98	0.0377
RB0204S2	0.0378	0.0399	0.95	0.03885
RB0204S3	0.0387	0.0398	0.97	0.03925
RB0205S1	0.0403	0.0421	0.96	0.03925
RB0121S1	0.0375	0.0417	0.90	0.0396
RB0121S3	0.0376	0.0403	0.93	0.03895

Rn-222 activity is based on the average values of Pb-214 and Bi-214 (radon progeny)

Reproduced with permission of the copyright owner. Further reproduction prohibited without permission.

Table 3.12: Statistics of Native Materials Gamma Spectroscopy for Radon Calculations (First-Round Sampling): n = 7

Radionuclide	Low Activity ($Bq\ g^{-1}$)	High Activity ($Bq\ g^{-1}$)	Average Activity ($Bq\ g^{-1}$)	Standard Deviation
Pb-214	0.0374	0.0403	0.0382	0.0011
Bi-214	0.0380	0.0421	0.0392	0.0016
Rn-222	0.0377	0.0396	0.0383	0.0009
(Pb214/Bi214)	0.90	0.98	0.96	0.036

Table 3.13: The Calculated Activity of Radon From its Progeny, Gamma Spectroscopy of Native Material Samples from In-Situ Sampling Location:

Sample #	Pb-214 ($Bq\ g^{-1}$)	Bi-214 ($Bq\ g^{-1}$)	Ratio (Pb-214/Bi-214)	Rn-222 ($Bq\ g^{-1}$)
RB0407S1	0.0384	0.0396	0.970	0.0390
RB0407S2	0.0333	0.0395	0.843	0.0364
RB0407S3	0.0388	0.0402	0.965	0.0395
RB0407S4	0.0378	0.0393	0.961	0.0386
RB0407S5	0.0369	0.0384	0.961	0.0377
RB0407S6	0.0362	0.0388	0.933	0.0375

Rn-222 activity is based on the average values of Pb-214 and Bi-214 (radon progeny

Sample RB0407S2 gamma spectroscopy showed interferences for various radionuclides that other samples were able to be determined

Reproduced with permission of the copyright owner. Further reproduction prohibited without permission.

Table 3.14: Statistics of Native Materials (for In-Situ Sampling Location) Gamma Spectroscopy: n = 6

Radionuclide	Low Activity ($Bq\ g^{-1}$)	High Activity ($Bq\ g^{-1}$)	Average Activity ($Bq\ g^{-1}$)	Standard Deviation
Pb-214	0.0333	0.0388	0.0369	0.0020
Bi-214	0.0384	0.0402	0.0393	0.0006
Rn-222	0.0364	0.0395	0.0381	0.0011
(Pb214/Bi214)	0.84	0.97	0.94	0.049

Table 3.15: The Calculated Activity of Radon From its Progeny, Gamma Spectroscopy of Fiber Crete Samples - Dry

Sample #	Pb-214 ($Bq\ g^{-1}$)	Bi-214 ($Bq\ g^{-1}$)	Ratio (Pb-214/Bi-214)	Rn-222 ($Bq\ g^{-1}$)
RB0205F1	0.0155	0.0173	0.90	0.016
RB0205F2	0.0154	0.0175	0.88	0.017
RB0205F3	0.0146	0.0162	0.90	0.015
RB0205F4	0.0169	0.0182	0.93	0.018
RB0204F2	0.0161	0.0182	0.88	0.017

Rn-222 activity is based on the average values of Pb-214 and Bi-214 (radon progeny)

Reproduced with permission of the copyright owner. Further reproduction prohibited without permission.

Table 3.16: Statistics of Dry Fiber Crete Gamma Spectroscopy: n = 8

Radionuclide	Low Activity ($Bq\ g^{-1}$)	High Activity ($Bq\ g^{-1}$)	Average Activity ($Bq\ g^{-1}$)	Standard Deviation
Pb-214	0.0146	0.0169	0.0158	0.0004
Bi-214	0.0162	0.0182	0.01775	0.0006
Rn-222	0.0154	0.01755	0.0168	0.0005
(Pb214/Bi214)	0.88	0.93	0.89	0.008

Table 3.17: The Calculated Activity of Radon From its Progeny, Gamma Spectroscopy of Fiber Crete Samples Cured Material - Uncorrected Activity

Sample #	Pb-214 ($Bq\ g^{-1}$)	Bi-214 ($Bq\ g^{-1}$)	Ratio (Pb-214/Bi-214)	Rn-222 ($Bq\ g^{-1}$)
RB0311-01C	0.0109	0.0121	0.901	0.0115
RB0311-02C	0.0118	0.0131	0.901	0.0125
RB0311-03C	0.0112	0.0123	0.911	0.0118
RB0311-04C	0.0109	0.0119	0.916	0.0114
RB0311-05C	0.0114	0.0128	0.891	0.0121
RB0311-06C	0.0110	0.0122	0.902	0.0116

Reproduced with permission of the copyright owner. Further reproduction prohibited without permission.

Table 3.18: Statistics of Cured Fiber Crete Gamma Spectroscopy (Uncorrected Activity): n = 6

Radionuclide	Low Activity ($Bq\ g^{-1}$)	High Activity ($Bq\ g^{-1}$)	Average Activity ($Bq\ g^{-1}$)	Standard Deviation
Pb-214	0.0109	0.0118	0.0112	0.0004
Bi-214	0.0119	0.0131	0.0124	0.0005
Rn-222	0.0114	0.0125	0.0118	0.0004
(Pb214/Bi214)	0.89	0.92	0.90	0.0088

Table 3.19: The Calculated Activity of Radon From its Progeny Gamma Spectroscopy of Fiber Crete Samples Cured Material - Corrected Activity

Sample #	Pb-214 ($Bq\ g^{-1}$)	Bi-214 ($Bq\ g^{-1}$)	Ratio (Pb-214/Bi-214)	Rn-222 ($Bq\ g^{-1}$)
RB0311-01C	0.0131	0.0145	0.903	0.0138
RB0311-02C	0.0141	0.0157	0.898	0.0149
RB0311-03C	0.0134	0.0148	0.905	0.0141
RB0311-04C	0.0131	0.0144	0.910	0.0138
RB0311-05C	0.0137	0.0153	0.895	0.0145
RB0311-06C	0.0132	0.0146	0.904	0.0139

Reproduced with permission of the copyright owner. Further reproduction prohibited without permission.

Table 3.20: Statistics of Cured Fiber Crete Gamma Spectroscopy (Corrected Activity): n = 6

Radionuclide	Low Activity ($Bq\ g^{-1}$)	High Activity ($Bq\ g^{-1}$)	Average Activity ($Bq\ g^{-1}$)	Standard Deviation
Pb-214	0.0131	0.0141	0.0134	0.0004
Bi-214	0.0144	0.0157	0.0149	0.0005
Rn-222	0.0138	0.0149	0.0142	0.0004
(Pb214/Bi214)	0.90	0.91	0.90	0.0053

Table 3.21: A Comparison of Physical Data of Pre and Post Cure Fiber Crete Samples (Based on 1 Liter of Industrial Water Used During Mixing Process)

Sample #	Pre-Cure Weight (grams)	% of Sum	Cured Weight	% of Sum	Water loss between Pre and Post Cured (grams)
RB0311-01C	1046.0	16.4	1024.8	16.4	21.2
RB0311-02C	1057.4	16.6	1036.8	16.6	20.6
RB0311-03C	1069.3	16.8	1045.8	16.7	23.5
RB0311-04C	1090.0	17.1	1071.1	17.1	18.9
RB0311-05C	1054.2	16.5	1034.6	16.6	19.6
RB0311-06C	1055.5	16.6	1034.5	16.6	21.0
Σ	6372.4	100	6247.6	100	124.8

A comparison of the physical properties of First Round and In-Situ native material samples, as shown in Tables 3.1 and 3.2, indicate strong similarities between the two materials. The densities of these materials differed slightly with the First Round samples ranging from 1.28 - 1.35 g cm^{-3}, with an average of 1.32 ± 0.022, while the "In-Situ" lot ranged from 1.20 - 1.31, with an average of 1.24 ± 0.040 g cm^{-3}. Differences in density may be attributed to variations in measurement techniques employed for the two sample rounds. The first round sample volumes were performed by visually aligning the sample material to a drawn line on the 500-ml HDPE bottle, followed by filling the native material to the line. The second lot samples were measured with a graduated beaker prior to pouring the material into the bottle.

Gamma spectroscopy analysis for the First Round native materials resulted in activities ranging from 0.0380 - 0.0421 Bq g^{-1} for ^{214}Bi and 0.0374 - 0.0403 Bq g^{-1} for ^{214}Pb. Their respective averages were 0.0392 ± 0.00163 Bq g^{-1} and 0.0382 ± 0.00112 Bq g^{-1}. Calculating the amount of radon from these activities, based on the assumption of equilibrium, shows an activity concentration of 0.0383 ± 0.00088 Bq g^{-1} (ranging from 0.0377 - 0.0396 Bq g^{-1}). The specific radon activity was obtained by the average activities of ^{214}Pb and ^{214}Bi.

Gamma spectroscopy analysis for the "In-Situ" native materials resulted in very similar activities to the first round samples. In-situ activities ranged from 0.0384 - 0.0402 Bq g^{-1} for ^{214}Bi and 0.0333 - 0.0388 Bq g^{-1} for ^{214}Pb. Their respective averages were 0.0393 ± 0.0006 Bq g^{-1} and 0.0369 ± 0.0020 Bq g^{-1}. Calculating the amount of radon

Reproduced with permission of the copyright owner. Further reproduction prohibited without permission.

from these activities, resulted in an activity of 0.0381 ± 0.0011 Bq g^{-1} (ranging from 0.0364 - 0.0395 Bq g^{-1}).

The gamma spectroscopy analysis for the fiber crete samples measured the ranges for ^{214}Bi and ^{214}Pb as 0.0144 - 0.0157 Bq g^{-1} and 0.0131 - 0.0141 Bq g^{-1}, respectively. Their averages and standard deviations were calculated to be 0.0149 ± 0.0005 Bq g^{-1} for ^{214}Bi and 0.0134 ± 0.0004 Bq g^{-1} for ^{214}Pb. These activity concentrations translate to an average radon activity concentration of 0.0142 ± 0.0005 Bq g^{-1}, with a range of 0.0138 - 0.0149 Bq g^{-1}.

Gamma spectroscopy of the industrial water, used to mix the cured the fiber crete at U1a, resulted in activity concentrations for the radionuclides ^{214}Pb, ^{214}Bi and ^{234}Th, that were less than their respective minimum detectable activity (MDA). This suggests that the industrial water did not influence the cured fiber crete radon activity concentration. Table 3.5 lists the industrial water gamma spectroscopy results.

A comparison of the two native material lots' activity concentrations show strong similarities for the radionuclides detected (Tables 3.6 and 3.7), including their respective radon activities. Tables 3.11 - 3.14 shows that the average ^{222}Rn activity to be 0.0383 ± 0.0009 Bq $g^{-1}$and 0.0381 ± 0.0011 Bq g^{-1} for the First Round and In-Situ material lots, respectively.

The activities of ^{214}Pb and ^{214}Bi were used to determine radon activity, as both these radionuclides showed distinct peaks and were easily quantified. Ratios of ^{214}Pb and ^{214}Bi were calculated as a method to quantify their similarities. The average activity concentration of each samples' ^{214}Pb and ^{214}Bi activities, were used as the actual activity

Reproduced with permission of the copyright owner. Further reproduction prohibited without permission.

concentration for radon. All samples (regardless of lot) showed a higher activity for ^{214}Bi, with average ratios of ^{214}Pb to ^{214}Bi of 0.96 and 0.94, for the First Round and In Situ locations, respectively. The lower ratio for the In Situ location was the result of sample RB0407S2, where the gamma spectroscopy resulted in a ^{214}Pb activity of 0.0333 Bq g^{-1}, and a $^{214}Pb/^{214}Bi$ ratio of 0.843. The ratios of ^{214}Pb to ^{214}Bi indicated similar activity concentrations. Therefore, each was used to calculate the radon activity concentration for each sample.

3.2 Lucas Cell Analysis

The range of net counts for the four native material samples was 93 - 116 for 20 minutes counting times. This equates to net count rates ranging from 4.65 - 5.80 counts per minute (cpm), with standard deviations for these count rates ranging from 0.48 - 0.55. Standard deviations were calculated using the formula:

$$\sigma_{rate} = (R_{sample}/T_{sample} + R_{background}/T_{background})^{1/2} \qquad (3.1)$$

where: R_{sample} = sample count rate,

T_{sample} = sample count time,

$R_{background}$ = background count rate, and

$T_{background}$ = background count time.

The range of net counts for the cured fiber crete samples was 848 - 1900, with a net count rate of 42.0 - 95.0 cpm and standard deviations ranging from 1.46 - 2.18. The net count range for the dry fiber crete was 71 - 255. Omitting sample RB0205F1 (cell #1)

Reproduced with permission of the copyright owner. Further reproduction prohibited without permission.

the range tightened to 160 - 255. The net count rate range was 3.6 - 12.8 cpm with a standard deviation of 2.00 - 3.6, including the cell #1 sample, and 8.0 - 12.8 cpm with a standard deviation of 2.9 - 3.6, without cell #1.

Tables 3.22 - 3.27 contain data pertaining to the emanation determination for In-Situ native materials, cured and dry fiber crete. Specific data included each material's emanation coefficient, gross and net counts, net count rate, and activity per unit mass, expressed as Bq g^{-1}. The native material had an emanation activity ranging from 0.18 – 0.24 mBq g^{-1}. The cured fiber crete ranged from 0.59 – 0.15 mBq g^{-1}. The dry fiber crete range was 0.085 – 0.28 mBq g^{-1}. It should be noted that the dry fiber crete sample, RB0205F1, yielded an activity concentration of 0.085 mBq g^{-1} (Table 3.27). This activity was not included in the final analysis due to sample error (refer to the "Discussion" section). Excluding this sample, the dry fiber crete emanation ranged from 0.18 to 0.28 mBq g^{-1}.

The average enamation for the native materials was 0.20 mBq g^{-1} and 0.6 mBq g^{-1} for the cured fiber crete, while the dry fiber crete had an average emanation of 0.19 mBq g^{-1} (including sample RB0205FI) and 0.21 mBq g^{-1} (omitting RB0205F1).

The emanation coefficients were calculated by dividing the emanation activity concentrations by the radon activity concentrations obtained during gamma spectroscopy. The emanation coefficients for the native materials ranged from 0.0047 - 0.0061: low

Reproduced with permission of the copyright owner. Further reproduction prohibited without permission.

Reproduced with permission of the copyright owner. Further reproduction prohibited without permission.

Table 3.22: Lucas cell Information for Native Materials Emanation Coefficient Determination: Date: 6/13/00

Cell #	Cell Efficiency (cpm dpm^{-1})	Cell Calibration Date	Cell Background Count (20 Minutes)
1	2.27	11/10/099	3
2	2.43	11/8/99	0
3	2.34	11/8/99	2
4	2.44	11/10/99	3

Table 3.23: Results of Lucas Cell Analysis for Native Material Emanation Coefficient (20 Minute Count Time): Date: 6/13/00

Sample #	Cell #	Sample Wt (Grams)	Gross Counts	Net Counts	Net Count Std Dev	Lucas Cell CPM	Lucas Cell DPM	Total sample DPM	Bq g^{-1}	Gamma Spec (Bq g^{-1})	Emanation Coefficient
RB0407S1	1	612.9	107	104	0.524	5.20	2.29	7.81	0.00021	0.0390	0.0054
RB0407S2	2	609.5	93	93	0.481	4.65	1.91	6.53	0.00018	0.0364	0.0049
RB0407S3	3	598.7	118	116	0.548	5.80	2.48	8.45	0.00024	0.0395	0.0061
RB0407S4	4	621.0	101	98	0.510	4.90	2.01	6.85	0.00018	0.0386	0.0047

Reproduced with permission of the copyright owner. Further reproduction prohibited without permission.

Table 3.24: Lucas cell Information for Cured Fiber Crete Emanation Coefficient Determination: Date: 6/21/00

Cell #	Cell Efficiency (cpm dpm^{-1})	Cell Calibration Date	Cell Background Count (20 Minutes)
1	2.27	11/10/099	1
2	2.43	11/8/99	4
3	2.34	11/8/99	2
4	2.44	11/10/99	3

Table 3.25: Results of Lucas Cell Analysis for Cured Fiber Crete Emanation Coefficient (20 Minute count Time): Date: 6/21/00

Sample #	Cell #	Sample Wt (Grams)	Gross Counts	Net Counts	Net Count Std Dev	Lucas Cell (cpm)	Lucas Cell (dpm)	Total sample dpm	Bq g^{-1}	Gamma Spec Bq g^{-1}	Emanation Coefficient
RB0311-01C	1	1024.8	943	942	1.54	47.1	31.12	47.3	0.00077	0.0138	0.056
RB0311-02C	2	1036.8	1904	1900	2.18	95.0	59.03	92.9	0.0015	0.0149	0.101
RB0311-03C	3	1045.8	1178	1176	1.72	59.0	38.07	56.8	0.00090	0.0141	0.064
RB0311-04C	4	1071.1	851	848	1.46	42.0	26.00	38.2	0.00059	0.0138	0.043

Reproduced with permission of the copyright owner. Further reproduction prohibited without permission.

Table 3.26: Lucas cell Information for Dry Fiber Crete Emanation Coefficient Determination: Date: 7/25/00

Cell #	Cell Efficiency (cpm dpm^{-1})	Cell Calibration Date	Cell Background Count (20 Minutes)
1	2.27	11/10/099	3
2	2.43	11/8/99	1
3	2.34	11/8/99	4
4	2.44	11/10/99	1
5	2.28	11/7/99	2

Table 3.27: Results of Lucas Cell Analysis for Fiber Crete (Dry) Emanation Coefficient (20 Minute Count Time): Date: 7/25/00

Sample #	Cell #	Sample Wt (grams)	Gross Counts	Net Counts	Net Count Std Dev	Lucas Cell cpm	Lucas Cell dpm	Total Sample dpm	Bq g^{-1}	Gamma Spec Bq g^{-1}	Emanation Coefficient
RB0205F1	1	869.7	74	71	1.96	3.55	1.56	4.43	0.000085	0.0164	0.0052
RB0205F2	2	865.7	161	160	2.85	8.00	3.39	9.31	0.000179	0.0165	0.0108
RB0205F3	3	875.6	181	177	3.04	8.85	3.78	10.51	0.000200	0.0154	0.0130
RB0205F4	4	869.4	256	255	3.58	12.75	5.23	14.80	0.000284	0.0176	0.0161
RB0205F1	5	869.7	163	161	2.87	8.05	3.53	9.99	0.000191	0.0164	0.0116

when compared to the emanation coefficient of crushed rock at 0.084 (see Table 1.1) and significantly low when compared to general soils with typical emanation coefficients of 0.2 - 0.4 This will be discussed in detail in the "Discussion" section of this report.

The emanation coefficients for the cured fiber crete measured approximately ten times the value as that for the native materials, ranging from 0.043 - 0.101. The emanation coefficients for dry fiber crete measured 0.0052 - 0.0161, including the cell #1 sample and 0.0108 - 0.0161 without the cell #1 sample.

While the initial net counts for the cured fiber crete appear to be much greater than those for the native material samples, the difference is reduced due to the larger head and void spaces of the native material samples. This is evident by the larger pressure drops with the native material during the transfer process of the emanated gas leaving the source material bottle to the lucas cell. Typical pressure drops for the native material transfer process was 19 mm Hg (27 to 8 mm Hg). This corresponds to an air volume of 241 centimeters cubed (cm^3), in addition to the 100 cm^3 lucas cell volume. The average pressure drop for the cured fiber crete samples was 8 mm Hg (from 27 to 19 mm Hg). This corresponds to an additional air volume of approximately 50 cm^3. For the dry fiber crete, the pressure drop was approximately 17 mm Hg (from 27 mm Hg to 10 mm Hg).

The air volumes measured via pressure drop were verified by a simple experiment consisting of saturating representative samples of all three materials with water until free product (i.e. liquid water) was observed. While no saturation was observed for the cured fiber crete sample, suggesting minimal void spaces, the native material showed 130 cm^3 of void space. For a 500 ml sample, this equates to 26% void space. Next, the head space was measured by observing the amount of water that filled the head space. This

Reproduced with permission of the copyright owner. Further reproduction prohibited without permission.

resulted in 96 ml for the native material sample and 70 ml for the cured fiber crete sample. The combined head space and void space for the native material sample calculated to 226 ml; very close to the space calculated via Boyle's Law of 236 cm^3. The total head space of the cured fiber crete sample was 50 cm^3; also fairly close to that total space of 70 ml obtained via pressure drops during emanating gas transfer. The dry fiber crete sample measured a head space of 100 ml, and a void space of 88 ml, totaling 188 ml. Again, close to the Boyle's law calculated value of 178 ml.

These total volumes were used to calculate the volume ratios of total sample space to Lucas cell space. This ratio was then multiplied by the "Lucas Cell dpm" to achieve the total sample dpm. These activities were recorded in Tables 3.23, 3.25, and 3.27 under "Lucas Cell dpm" and "Total Sample dpm" columns. The calculated ratio for the native material samples was 3.41. The ratio for the cured fiber crete samples was 1.50, while the dry fiber crete ratio was 2.83.

3.3 Exhalation - Charcoal Canisters

Two rounds for in-situ exhalation rates were conducted. Results are listed in Tables 3.28 - 3.37. Tables 3.28 - 3.32 display data for the first round, while Tables 3.33 - 3.37 display second round data. Figure 3.1 is a comparitive illustration of native material and fiber crete exhalation rates for the three sampling periods.

First round airborne concentrations involved sampling periods of approximately 3½ , 7, and 10 days (84, 171 and 252 hours). Laboratory results were reported in units of pCi l^{-1}.

Reproduced with permission of the copyright owner. Further reproduction prohibited without permission.

Reproduced with permission of the copyright owner. Further reproduction prohibited without permission.

Table 3.28: In-Situ Passive Diffusion Charcoal Canister Results: First-Round Sampling (Native Material)

Sample #	Exposure Time (Hours)	Total Counts	Background Counts	Detector Efficiency	DPM	Bq cm^{-2} hr^{-1}
11N	84	1600	108.1	0.3097	167.6	0.000405
21N	84	1576	108.2	0.3101	159.3	0.000393
31N	84	1571	104.5	0.2977	176.7	0.000429
41N	84	1681	113.1	0.3048	180.4	0.000440
51N	84	1544	104.3	0.3033	165.2	0.000405
61N	84	1754	104.9	0.3078	229.0	0.000560
71N	84	1676	111.9	0.3108	179.2	0.000440
01N	Blank	1099	118.5	0.3075	(-28.0)	N/A
12N	171	12126	108.1	0.3097	3538.0	0.00429
22N	171	10577	108.2	0.3101	3063.2	0.00368
32N	171	11856	104.5	0.2977	3624.5	0.00436
42N	171	12870	113.1	0.3048	3850.0	0.00463
52N	171	12044	104.4	0.3033	3631.7	0.00437
62N	171	12285	104.9	0.3078	3651.7	0.00439
72N	171	11076	111.9	0.3108	3204.3	0.00385
02N	Blank	1109	118.5	0.3075	(-28.6)	N/A
13N	252	5450	107.6	0.3097	1407.2	0.00115
23N	252	5495	107.8	0.3101	1419.9	0.00116
33N	252	5206	106.6	0.2977	1381.9	0.00113
43N	252	5148	113.5	0.3048	1330.7	0.00109
53N	252	5735	102.9	0.3033	1530.8	0.00125
63N	252	5595	104.5	0.3078	1463.0	0.00119
73N	252	5312	111.9	0.3108	1357.8	0.00111
03N	Blank	1164	119.7	0.3075	23.4	0.0000198

Reproduced with permission of the copyright owner. Further reproduction prohibited without permission.

Table 3.29: In-Situ Passive Diffusion Charcoal Canister Results First Round Sampling (Fiber Crete)

Sample #	Exposure Time (Hours)	Total Counts	Background Counts	Detector Efficiency	DPM	Bq cm^{-2} hr^{-1}
11C	84	1651	107.6	0.3097	183.7	0.000452
21C	84	1547	107.8	0.3101	150.0	0.000369
31C	84	1469	106.6	0.2977	142.4	0.000345
41C	84	1595	113.5	0.3048	152.2	0.000369
51C	84	1490	102.9	0.3033	147.4	0.000357
61C	84	1387	104.5	0.3078	109.8	0.000274
71C	84	1509	111.9	0.3108	125.5	0.000310
01C	Blank	1135	119.7	0.3075	(-16.3)	N/A
12C	171	13,297	109.2	0.3097	3946.0	0.00474
22C	171	9855	109.2	0.3101	2830.4	0.00340
32C	171	11372	109.2	0.2977	3461.9	0.00416
42C	171	10745	109.2	0.3048	3152.9	0.00379
52C	171	11083	109.2	0.3033	3314.9	0.00398
62C	171	10819	109.2	0.3078	3175.4	0.00382
72C	171	11571	109.2	0.3108	3362.9	0.00404
02C	Blank	1160	109.2	0.3075	(-12.0)	N/A
13C	252	6309	109.2	0.3097	1684.5	0.00137
23C	252	5239	109.2	0.3101	1337.3	0.00109
33C	252	5551	109.2	0.2977	1497.8	0.00122
43C	252	5607	109.2	0.3048	1481.3	0.00121
53C	252	5703	109.2	0.3033	1520.3	0.00124
63C	252	5500	109.2	0.3078	1432.1	0.00119
73C	252	5528	109.2	0.3108	1427.3	0.00119
03C	Blank	1209	109.2	0.3075	38.0	0.0000317

Reproduced with permission of the copyright owner. Further reproduction prohibited without permission.

Table 3.30: Passive Diffusion Charcoal Canister Statistics: First Round Sampling (pCi L^{-1})

	84 Hrs	84 Hrs	171 Hrs	171 Hrs	252 Hrs	252 Hrs
	Native Mat.	Fiber Crete	Native Mat	Fiber Crete	Native Mat	Fiber Crete
	2.90	3.20	28.30	32.00	10.39	12.43
	2.70	2.60	24.30	22.90	10.48	9.87
	3.00	2.50	28.80	28.00	10.20	11.05
	3.10	2.60	30.50	25.50	9.82	10.93
	2.80	2.50	28.80	26.90	11.30	11.22
	3.90	1.90	29.00	25.70	10.80	10.57
	3.10	2.20	25.40	27.20	10.02	10.53
sum	21.50	17.50	195.10	188.20	73.01	76.6
ave	3.07	2.50	27.87	26.89	10.43	10.94
stdev	0.39	0.40	2.20	2.79	0.498	0.792

Table 3.31: Passive Diffusion Charcoal Canister Statistics: First Round Sampling (Bq cm^{-2} hr^{-1})

	84 Hrs	84 Hrs	171 Hrs	171 Hrs	252 Hrs	252 Hrs
	Native Mat.	Fiber Crete	Native Mat	Fiber Crete	Native Mat	Fiber Crete
	0.000405	0.000452	0.00429	0.00474	0.00115	0.00137
	0.000393	0.000369	0.00368	0.00340	0.00116	0.00109
	0.000429	0.000345	0.00436	0.00416	0.00113	0.00122
	0.000440	0.000369	0.00463	0.00379	0.00109	0.00121
	0.000405	0.000357	0.00437	0.00398	0.00125	0.00124
	0.000560	0.000274	0.00439	0.00382	0.00119	0.00119
	0.000440	0.000310	0.00385	0.00404	0.00111	0.00119
sum	0.003072	0.002476	0.02957	0.02793	0.00808	0.00851
ave	0.000439	0.000354	0.00422	0.00399	0.00115	0.00122
stdev	0.000056	0.000055	0.00034	0.00041	0.00005	0.00008

Reproduced with permission of the copyright owner. Further reproduction prohibited without permission.

Reproduced with permission of the copyright owner. Further reproduction prohibited without permission.

Table 3.32: Passive Diffusion Charcoal Canister Results t-Test: Two-Sample Assuming Unequal Variances First-Round Sampling

	84-Hour Samples		171-Hour Samples		252-Hour Samples	
	Native Material	*Fiber Crete*	*Native Material*	*Fiber Crete*	*Native Material*	*Fiber Crete*
Mean	3.071429	2.5	27.87143	26.88571	10.43	10.94286
Variance	0.155714	0.16	4.825714	7.784762	0.2485	0.626757
Observations	7	7	7	7	7	7
Hypothesized Mean Difference	0		0		0	
df	12		11		10	
t Stat	2.690691		0.734403		-1.45037	
P(T<=t) one-tail	0.009822		0.239033		0.088794	
t Critical one-tail	1.782287		1.795884		1.812462	
P(T<=t) two-tail	0.019645		0.478067		0.177588	
t Critical two-tail	2.178813		2.200986		2.228139	

Reproduced with permission of the copyright owner. Further reproduction prohibited without permission.

Table 3.33: In-Situ Passive Diffusion Charcoal Canister Results (Native Material Surfaces) Second-Round Sampling

Sample #	Exposure Time (hours)	Total Counts	Background (cpm)	Detector Efficiency	DPM	Bq cm^{-2} hr^{-1}
14N	167	5631	105.6	0.3097	1477	0.00182
24N	167	5916	105.8	0.3101	1567	0.00193
44N	167	7104	113.9	0.3048	1957	0.00241
54N	167	6600	102.4	0.3033	1830	0.00226
64N	167	6129	100.4	0.3078	1665	0.00205
34N*	167	6977	104.8	0.2977	1992	0.00245
04B	Blank	990	102.8	0.3108	(-12.23)	N/A

* Sample 34N was left unsealed to the surface (not included with other samples for comparison to fiber crete surface)

Table 3.34: In-Situ Passive Diffusion Charcoal Canister Results (Fiber Crete Surfaces) Second-Round Sampling

Sample #	Exposure Time (hours)	Total Counts	Background (cpm)	Detector Efficiency	DPM	Bq cm^{-2} hr^{-1}
14C	167	3479	105.6	0.3097	782	0.00096
24C	167	2581	105.8	0.3101	491	0.00061
44C	167	4201	113.9	0.3048	1005	0.00124
54C	167	3920	102.4	0.3033	955	0.00118
64C	167	3224	100.4	0.3078	721	0.00089
34C*	167	6704	104.8	0.2977	1900	0.00234
04B	Blank	990	102.8	0.3108	(-12.23)	N/A

* Sample 34C was left unsealed to the surface (not included with other samples for comparison to Native Material surfaces)

Table 3.35: Passive Diffusion Charcoal Canister Statistics: Second-Round Sampling (pCi l^{-1}): 167-Hour Sealed Canisters

	Fiber Crete Samples	Native Material Samples
	6.2	11.8
	3.9	12.5
	8.0	15.6
	7.6	14.7
	5.7	13.3
Sum	31.4	67.9
Average Value	6.28	13.58
Standard Deviation	1.64	1.56
Non-Sealed Samples	15.9	15.1

Reproduced with permission of the copyright owner. Further reproduction prohibited without permission.

Reproduced with permission of the copyright owner. Further reproduction prohibited without permission.

Table 3.36: Passive Diffusion Charcoal Canister Statistics: Second-Round Sampling (Bq cm^{-2} hr^{-1}): 167-Hour Sealed Canisters

	Native Material Samples	Fiber Crete Samples
	0.00182	0.00096
	0.00193	0.00061
	0.00241	0.00124
	0.00226	0.00118
	0.00205	0.00089
Sum	**0.01047**	**0.00488**
Average Value	**0.00209**	**0.00099**
Standard Deviation	**0.00024**	**0.00025**
Non-Sealed Samples	**0.00245**	**0.00234**

Reproduced with permission of the copyright owner. Further reproduction prohibited without permission.

Table 3.37: Passive Diffusion Charcoal Canister Results (Excel Spreadsheet) t-Test: Two-Sample Assuming Unequal Variances Second-Round Sampling (Based on EPA Laboratory Results of pCi l^{-1})

	167-Hour Samples	
	Fiber Crete	Native Material
Mean	6.28	13.58
Variance	2.677	2.437
Observations	5	5
Hypothesized Mean Difference	0	
df	8	
t Stat	-7.21	
P(T<=t) one-tail	4.54E-05	
t Critical one-tail	1.86	
P(T<=t) two-tail	9.08E-05	
t Critical two-tail	2.31	

Reproduced with permission of the copyright owner. Further reproduction prohibited without permission.

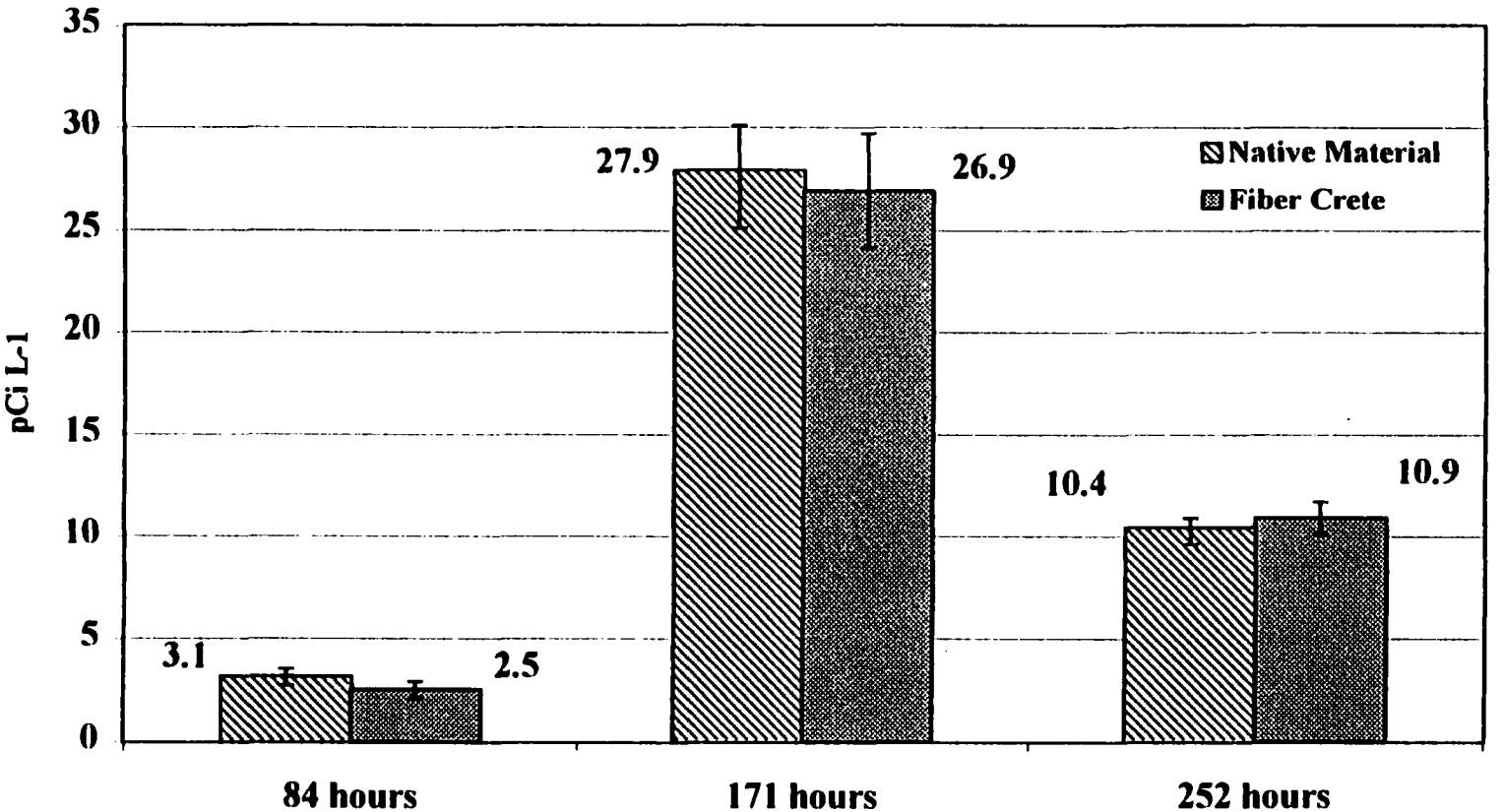

Figure 3.1 A Comparison of Native Material and Fiber Crete Exhalation Rates During the First Round of Sampling

The first round in-situ placement of the passive absorption charcoal canisters resulted in an average value for 3 ½ day (84 hour) collection of 2.5 ± 0.4 pCi l^{-1} on the fiber crete surface and 3.07 ± 0.4 pCi l^{-1} for the native material surface. The seven values of the fiber crete surface ranged from 1.9 - 3.2 pCi l^{-1}, while the native material surface resulted in a range from 2.7 - 3.9 pCi l^{-1}.

The seven day collection periods (171 hours) resulted in an average value for the fiber crete surface at 26.9 pCi l^{-1}, ranging from 22.9 - 32.0 pCi l^{-1}, with a standard deviation of 2.8. The results for the canisters placed on the native material for 171-hours showed an average value of 27.9 pCi l^{-1}, ranging from 24.3 - 30.5 pCi l^{-1} and a standard deviation of 2.2.

Samples collected for 10-day periods (252 hours) initially were not analyzed, as the collection time was greater than the laboratory sampling time criteria. Raw data (counts, sampling time and background counts) were still detected and a manual calculation was performed. Results indicate an average activity for the fiber crete surface was 10.9 pCi l^{-1}, ranging from 9.9 to 12.4, with a standard deviation of 0.8. The results for the canisters placed on the native material surface showed an average concentration of 10.4 pCi l^{-1}, ranging from 9.8 to 11.3, with a standard deviation of 0.5.

The exhalation values that the EPA lab reported in pCi l^{-1}, were modified by using the raw counting data, to determine the amount of activity (due to radon gas) associated with the sampled surfaces. These values are based on the net counts (gross counts minus the background) which were then divided by the detector efficiency. Each sample was blank corrected by subtracting the blank sample net counts. Next, the

Reproduced with permission of the copyright owner. Further reproduction prohibited without permission.

remainder was divided by the canister area of 81.07 cm^2 and the exposure time, resulting in a specific activity for each individual canister, expressed as activity exhalating per area per time (mBq cm^{-2} hr^{-1}).

84 hour collection samples for fiber crete surfaces showed an average exhalation activity of 0.354 ± 0.06 mBq cm^2 hr^{-1}, ranging from 0.27 – 0.45 mBq cm^{-2} hr^{-1}. Native material surface samples showed an average value of 0.44 ± 0.06 mBq cm^{-2} hr^{-1} with a range from 0.39 – 0.56 mBq cm^{-2} hr^{-1}.

171-hour samples for fiber crete surfaces showed an average exhalation activity of 4.0 ± 0.4 mBq cm^{-2} hr^{-1}, ranging from 3.4 – 4.7 mBq cm^{-2} hr^{-1}. Native material surface samples showed an average value of 4.2 ± 0.34 mBq cm^{-2} hr^{-1} ranging from 3.7 – 4.6 mBq cm^{-2} hr^{-1}.

252-hour samples for fiber crete surfaces showed an average activity of 1.22 ± 0.08 mBq cm^{-2} hr^{-1}, ranging from 1.1 – 1.4 mBq cm^{-2} hr^{-1}. Native material surface samples showed an average exhalation rate of 1.2 ± 0.05 mBq cm^{-2} hr^{-1} with a range from 1.1 – 1.3 mBq cm^{-2} hr^{-1}.

A second round of passive diffusion charcoal canisters was conducted due to the unexpected results from the first round sampling (refer to the "Discussion" section). Environmental data showed that the ventilation system was shut off for approximately two days. In addition, the canisters were not sealed to the surfaces, possibly allowing radon from the ambient environment, rather than the exhalating surfaces, to adhere onto the charcoal in addition to the exhalated radon.

Reproduced with permission of the copyright owner. Further reproduction prohibited without permission.

The second round of sampling was supported by U1a management and the EPA. Sampling locations were the same as the first round. A total of thirteen canisters were provided by the EPA: six were placed on the fiber crete surface and six on the native material surface. The thirteenth canister served as a blank. For each surface, five of the six canisters were sealed with clay to prevent any ambient radon activity from entering into the canister. Therefore only radon exhalating from the surface material should enter the canister's charcoal surfaces. Figure 3.2 shows how the First Round sampling canisters were placed on the rib surfaces without a tight seal between canister and rib surface. Figure 3.3 shows the canister placement for the Second Round sampling with a tight seal around the canister. The sixth canister for each surface was left unsealed, similar to the canisters used in the first round of sampling. If the two unsealed canisters (one on the fiber crete surface and the other on the native material surface) resulted in similar activities, while being significantly different from the sealed canisters, it would be an indication that the activity measured from the first round samples were attributed mainly to ambient radon conditions from the drift environment, rather than radon exhalating from their respective surfaces.

Second round exhalation rate sampling was conducted for approximately seven days (167 hours). The recorded activity for the native material surface, using canisters sealed to the surface, ranged from 11.8 - 15.6 pCi l^{-1}. This equated to 0.0018 - 0.0024 Bq cm^{-2} hr^{-1}. The average exhalation rate was 13.6 ± 1.6 pCi l^{-1}, or 0.0021 ± 0.0002 Bq cm^{-2} hr^{-1}. Figure 3.4 is a comparative illustration of the second round exhalation rates for native material and fiber crete surfaces.

Reproduced with permission of the copyright owner. Further reproduction prohibited without permission.

Reproduced with permission of the copyright owner. Further reproduction prohibited without permission.

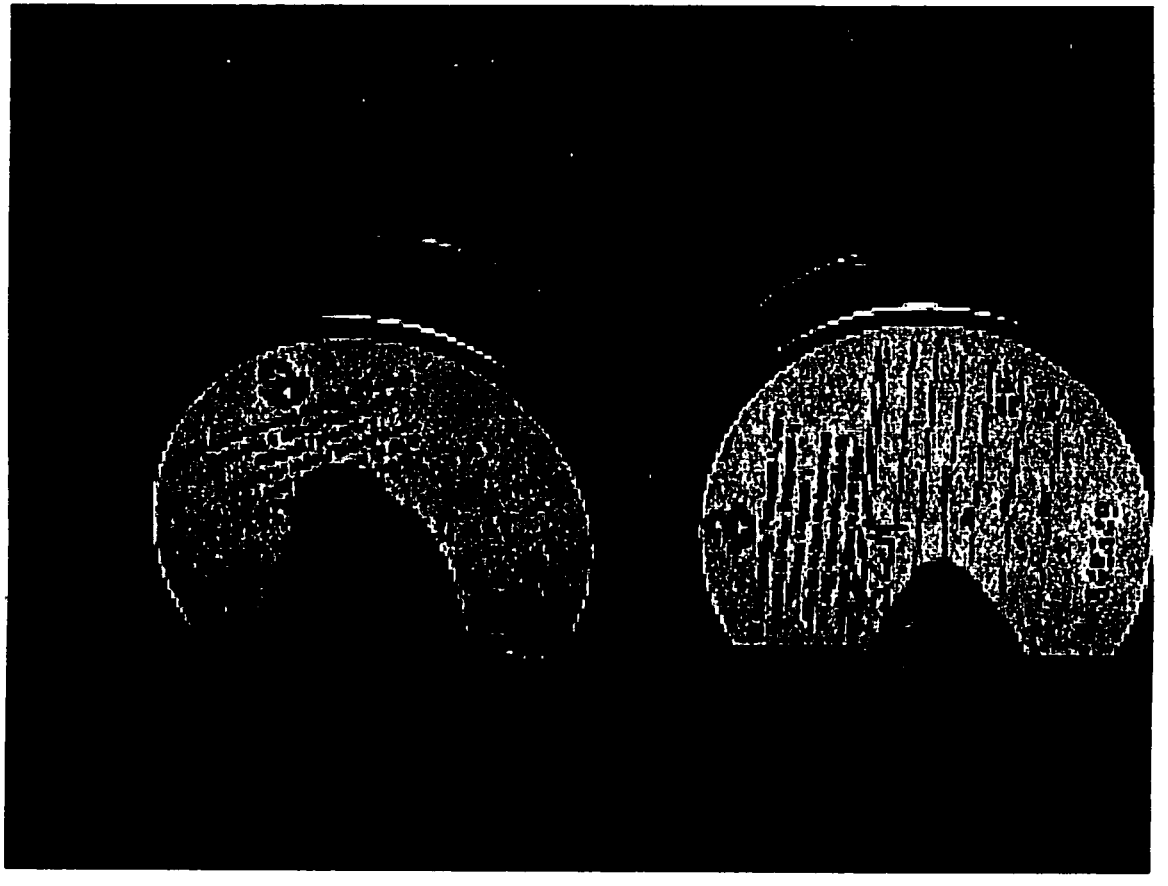

Figure 3.2 First Round In-Situ Sampling with Unsealed Canisters

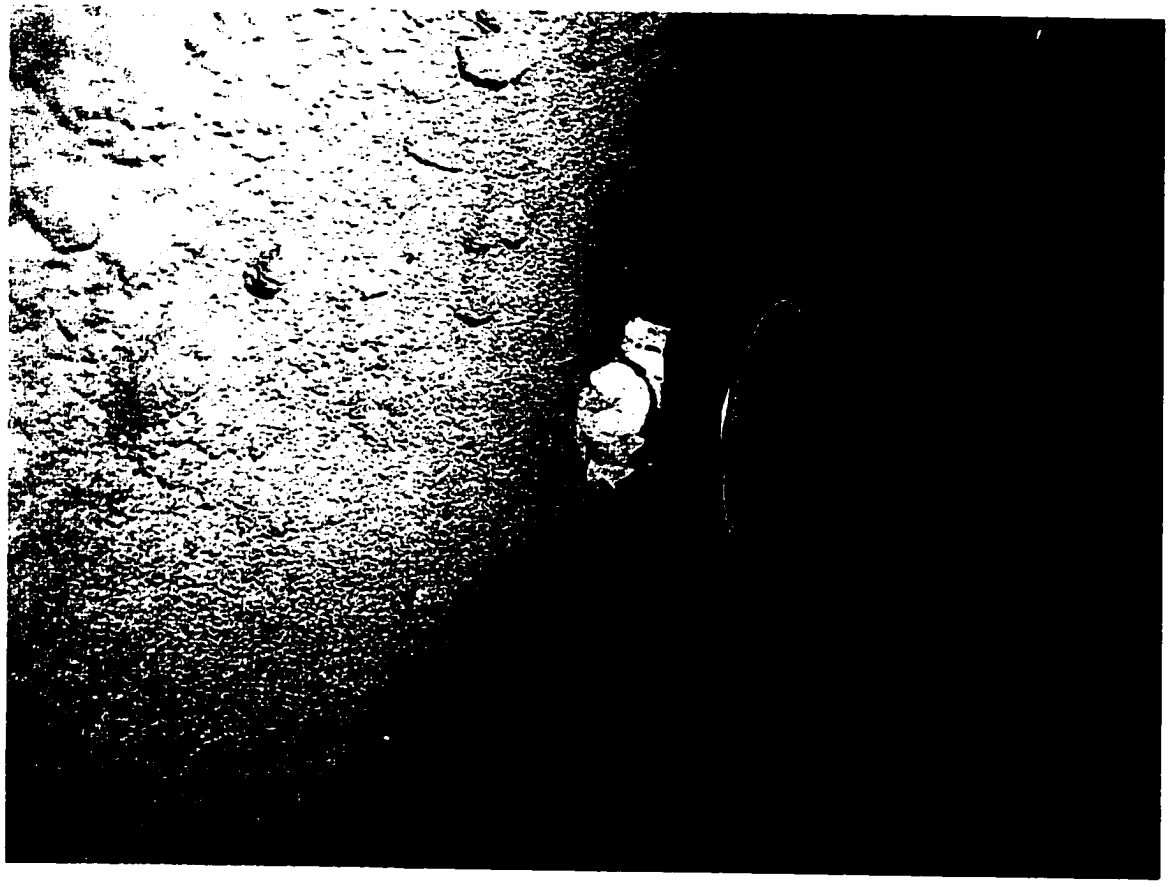

Figure 3.3 Second Round In-Situ Sampling with Sealed Canisters

Reproduced with permission of the copyright owner. Further reproduction prohibited without permission.

The fiber crete surfaces ranged from 3.9 - 8.0 pCi·L^{-1} with an average rate of 6.28 ± 1.6 pCi l^{-1} (refer to Figure 3.4). This converts to a range of 0.61 - 1.2 mBq cm^{-2} hr^{-1} and an average exhalation rate of 0.99 ± 0.25 mBq cm^{-2} hr^{-1}.

The two unsealed canisters, one for each surface, measured 15.1 pCi l^{-1} or 0.0025 Bq cm^{-2} hr^{-1} for the native material surface, and 15.9 pCi l^{-1} or 2.3 mBq cm^{-2} hr^{-1} for the fiber crete surface.

Reproduced with permission of the copyright owner. Further reproduction prohibited without permission.

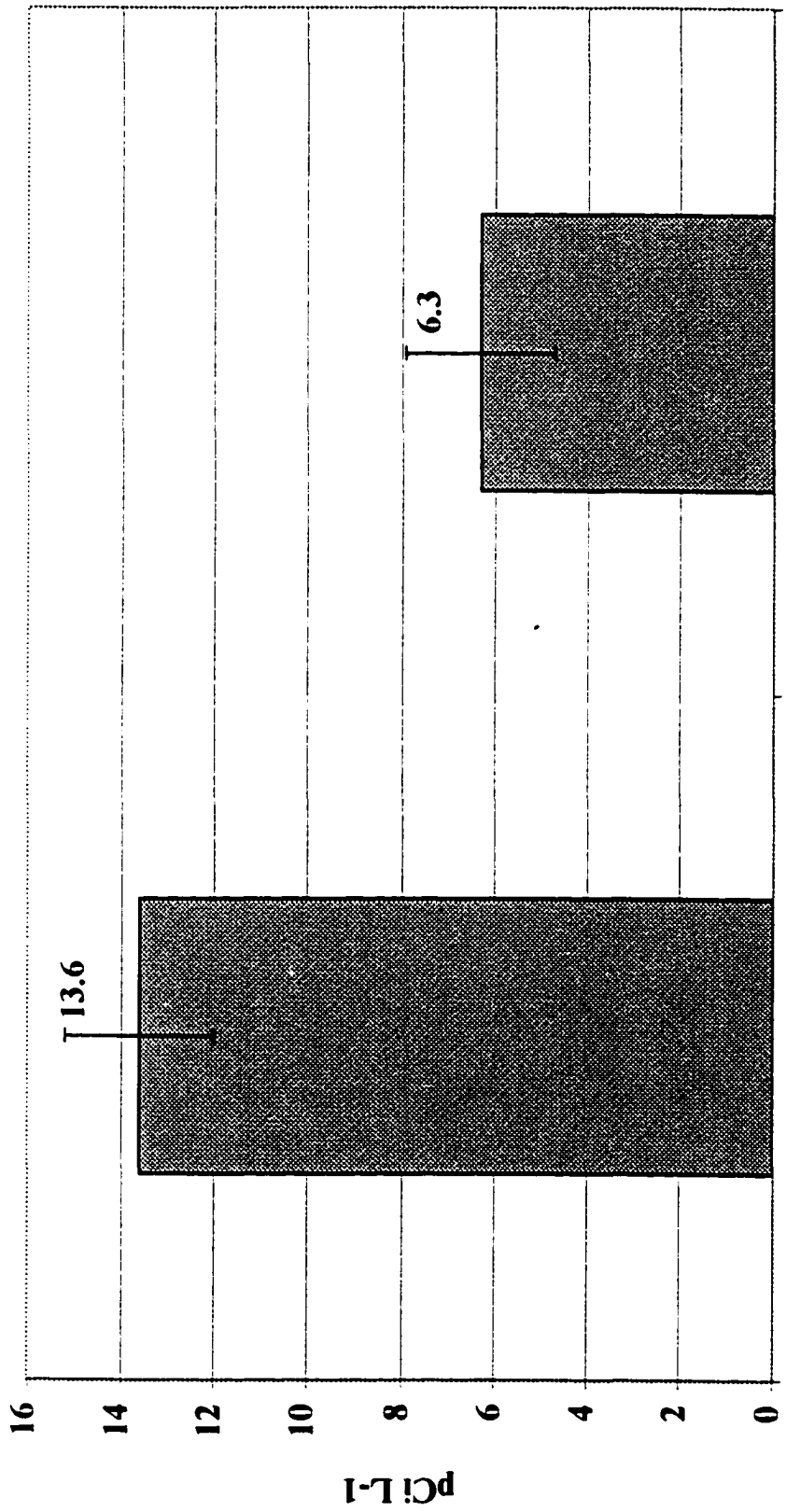

Figure 3.4. A Comparision of Native Material and Fiber Crete Exhalation Rates During the Second Round of Sampling.

Reproduced with permission of the copyright owner. Further reproduction prohibited without permission.

CHAPTER IV

DISCUSSION

4.1 Analysis of Native Materials and Fiber Crete

Radon activity was characterized by the direct relationship it has with its progeny, ^{214}Pb and ^{214}Bi. Like all relationships between radionuclides in the same decay chain, a direct quantification may only be assumed under equilibrium conditions. Therefore it was important that the gamma spectroscopy was conducted after a minimum of 7 half-lives (28 days) after sealing the 500-ml HDPE bottles prior to analysis. In addition to radon progeny, ^{234}Th was examined as an alternate method to quantify radon activity. Gamma spectroscopy results, displayed in Tables 3.6 and 3.7, show ^{234}Th activity to be higher than the activities of ^{214}Pb (0.0375 and 0.0369 Bq g^{-1}) and ^{214}Bi (0.0392 and 0.0393 Bq g^{-1}) for both first round and in-situ sampling. The average ^{234}Th activities for the first and in-situ round sampling of the native material was 0.0492 and 0.0472 Bq g^{-1}, respectively. The higher activity for ^{234}Th is related to the gamma spectroscopy calibration settings, which were designed for materials with densities of 1.5 g cm^{-3}. In addition, while equilibrium conditions were designed for quantification for radon and its progeny (minimum of 28 days), the longer half-lives of ^{234}Th (24 days) and ^{226}Ra (1620 years), could not be established during the time frame of this study, and

Reproduced with permission of the copyright owner. Further reproduction prohibited without permission.

therefore, possibly resulting in a misrepresentation of their activities. Figure 4.1 illustrates the activities of these three radionuclides for both native materials.

Verification that a direct relationship exists between ^{214}Pb and ^{214}Bi activities and ^{222}Rn and ^{226}Ra activities for each material sampled is critical. This relationship establishes the fundamental basis by which emanation coefficients and exhalation rates can be assessed. This is accomplished by comparing the gamma spectroscopy results to literature values. By assuming the sample decay products are in equilibrium with each other, the calculated ^{222}Rn activity is considered to be equal to ^{226}Ra. The calculated activity concentration of 0.038 Bq g^{-1} agrees with the established values for ubiquitous ^{226}Ra in soils of 30 - 70 Bg kg^{-1} (NCRP 1988). A study conducted by Luetzelschwab et al (1989), shows the radon concentration for five soils (sanstone, limestone, gray shale, red shale, and gneiss) ranging from 0.009 Bq g^{-1} to 0.104 Bq g^{-1} with an average concentration of 0.036 Bq g^{-1}. These activity concentrations agree with the calculations for radon activity based on the gamma spectroscopy results for ^{214}Pb and ^{214}Bi.

Results showed, without exception, the activity for ^{214}Bi was higher than that for ^{214}Pb. This inconsistency is due to interferences and calibration errors associated with the detection of the two radionuclides rather than any natural phenomenon of earthen materials. Ratios for these radionuclides were calculated for native materials and fiber crete and were compared to each other. Tables 3.12 and 3.14 show the $^{214}Pb/^{214}Bi$ ratio for native material ranges from 0.899 - 0.984 with an average value of 0.95 for the first round samples and 0.843 - 0.97 with an average value of 0.039 for the in-situ samples. The ratio range for dry fiber crete is 0.88 - 0.929 with an average value of 0.90.

Reproduced with permission of the copyright owner. Further reproduction prohibited without permission.

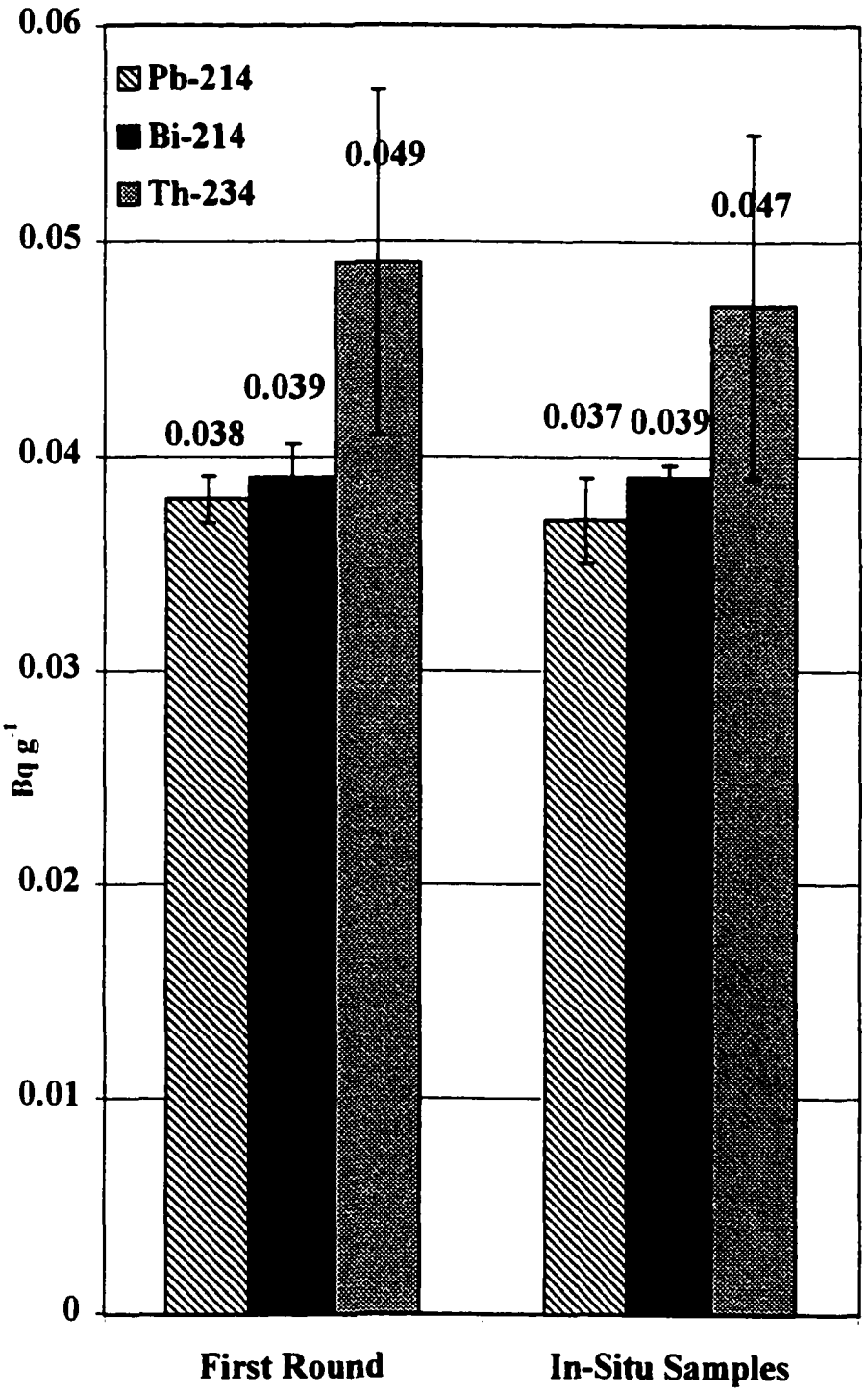

Figure 4.1 Activities for ^{214}Pb, ^{214}Bi and ^{234}Th for Native Material Samples

Reproduced with permission of the copyright owner. Further reproduction prohibited without permission.

This is the same for the cured fiber crete (water-corrected and uncorrected) (Tables 3.16, 3.18, and 3.20). Therefore the difference in activity detection between ^{214}Pb and ^{214}Bi is greater with the fiber crete samples, indicating a greater shift from the instrument calibration parameters.

Aside from density differences, the activity difference between these two radionuclides may be attributed to the higher gamma energies, at higher rates, produced for ^{214}Bi compared with ^{214}Pb. ^{214}Bi has major peaks at 0.609 (46.1 %), 1.12 MeV (15.0 %), 1.765 MeV (15.9 %), and 2.2 MeV (5.0 %), compared to peaks at 0.242 MeV (7.5 %), 0.295 MeV (19.2%), and 0.352 MeV (37.1) for ^{214}Pb. Therefore, the higher energies, at greater percentages, have a greater possibility to penetrate the distance through the medium and past the HDPE bottle.

The gamma spectroscopy results presented in Tables 3.6 - 3.10 include the uncertainties for each radionuclide for each material tested. These uncertainties represent one standard deviation, thus providing an indication of the activity's measure of dispersion or variability. Narrow distributions indicate that a measured activity has a low sampling variability, while wide distributions indicate high variability. While the native material uncertainties for ^{214}Bi were, in general, smaller than those for ^{214}Pb, both analytes had very similar uncertainty values of approximately 0.002 Bg g^{-1}. This suggests the measured activities for ^{214}Pb (average activity of 0.0375 Bg g^{-1}) and ^{214}Bi (average activity of 0.0392 Bg$\cdot$ gr^{-1}) have fairly narrow variations. The samples for cured fiber crete showed a leptokurtic (very narrow) distribution curve (compared to the native materials) for ^{214}Pb and ^{214}Bi activities. Typical uncertainties of 0.0004 indicate a very tight distribution for activities ranging from 0.0131 to 0.0141 (for ^{214}Pb) and 0.0144 to

Reproduced with permission of the copyright owner. Further reproduction prohibited without permission.

0.0157 (for ^{214}Bi). The distributions for both native materials and cured fiber crete indicate that the gamma spectroscopy data are within a narrow measure of variability and provide accurate activities, which, in turn, support using radon progeny to measure other parameters, such as, ^{226}Ra in soil, and the total ^{222}Rn activity.

Table 3.21 shows a comparison between the six cured fiber crete samples, pre and post cured, displaying the water loss for each sample. The results indicate that a total of 124.8 grams of water evaporated (from the original 1000 ml used to mix the six samples) during the cure process with an average weight loss of 16.7 % from each sample. There was an average addition of 146.2 grams of water to each sample. Most of the water formed a hydrate with the fiber crete material.

As a result of the water loss during the cure process, the activity detected by gamma spectroscopy needed to be corrected so a comparison could be made between the pre and post-cured fiber crete. Because the activity concentration of the industrial water is negligible, the total mass of each sample needed to be reduced to account for the activity being attributed only to the cured fiber crete. This was accomplished by dividing the recorded activities by the reduced sample mass of the fiber crete material only, resulting in a larger activity concentration. The resultant activity was used to calculate the emanation coefficient and percent exhalation for the cured fiber crete surfaces.

4.2 Lucas Cell Analysis via Scintillation Measurement

Figure 4.2 illustrates the average radon emanation coefficient for the three materials tested; In-situ native material, cured fiber crete, and dry fiber crete. The high

Reproduced with permission of the copyright owner. Further reproduction prohibited without permission.

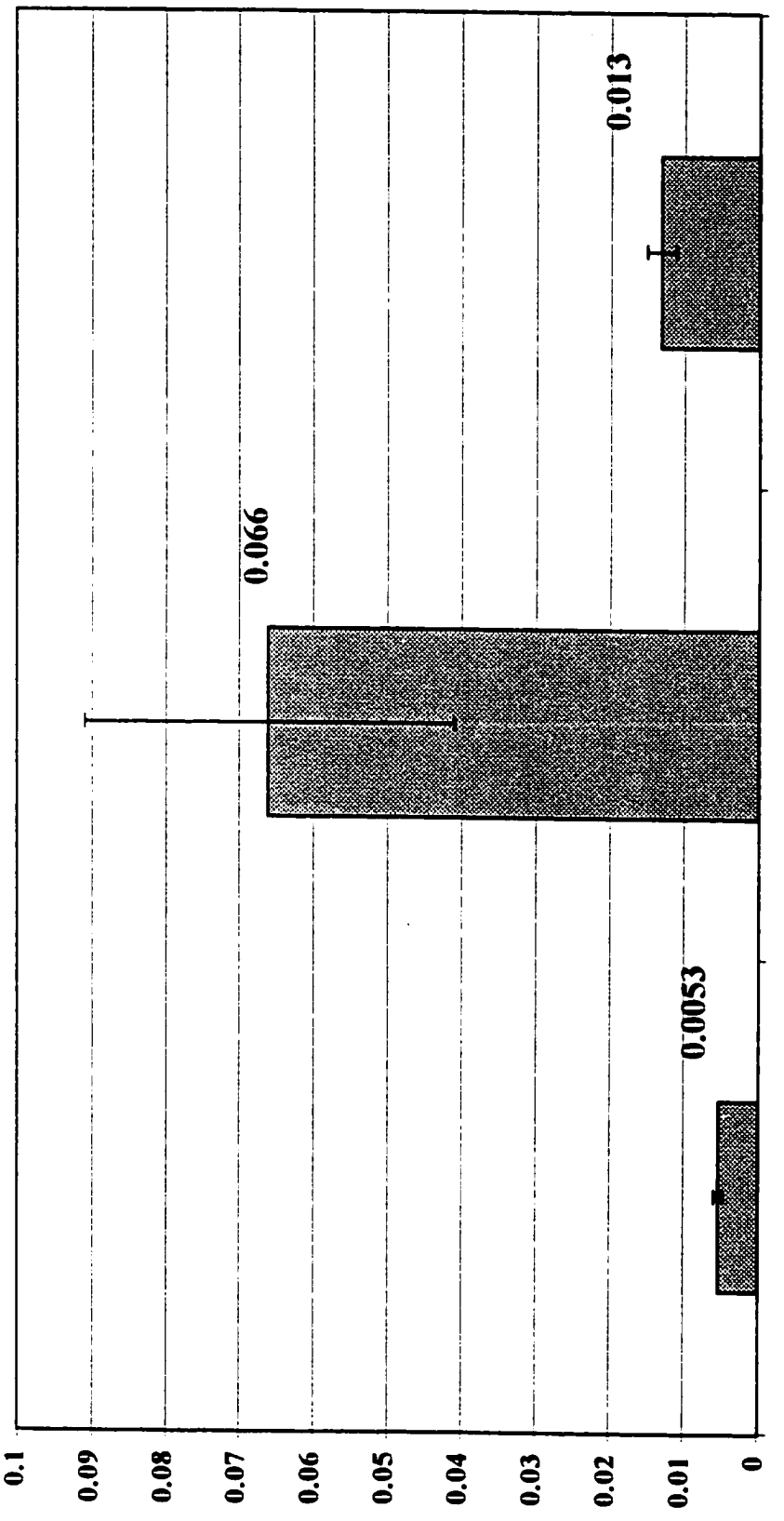

Figure 4.2. Emanation Coefficients for Native Material, Cured Fiber Crete and Dry Fiber Crete

Reproduced with permission of the copyright owner. Further reproduction prohibited without permission.

emanation coefficient for the cured fiber crete can be attributed to the material's moisture content and small pore size.

Table 2.1 shows the majority of native material within the nearby .03 drift of the U1a Complex consisting of over 60% sand. The remainder is composed of approximately 6% silt, 9% clay and 24% pebbles and cobbles. For this study, pebbles and cobbles are classified as gravels. The particle size distribution for the native material and fiber crete is listed in Table 4.1.

As noted in section 1.3, particle size plays an influential role in radon emanation. In addition, Luetzelschwab et al (1989), noted that soil densities also effect emanation, such that the more densely packed a soil is, the greater the emanation. This is attributed to a reduced interstitial air space and the greater grain surface area contact with the air space associated with the smaller particles. The densities of all samples, listed in Tables 3.1 - 3.5, show the densities of native materials to be approximately 1.3 g cm^{-3}, while those of the dry and cured fiber crete are 1.7 g cm^{-3} and 2.1 g cm^{-3}, respectively.

A comparison of a dry particle size distribution conducted in the work (see Table 4.1) confirms size distribution similarities for sand (62.5%), and pebbles and cobbles (29%) as shown in Table 2.1. Silts and clays, comprising 8.4%, were less than the distribution displayed in Table 2.1 (combined at 14.5%). This difference can be attributed to dry size distributions underestimating silt and clay composition as these constituents are not being completely dissolved and separated from the larger sand and gravel particles. A more complete separation method is a wet chemical particle distribution (Sheldrick 1993). Based on this premise, a wet distribution would have

Reproduced with permission of the copyright owner. Further reproduction prohibited without permission.

Table 4.1 Particle Size Distribution for Native Material and Fiber Crete

Particle Size	Native Material %	Fiber Crete %	Material Category
12.5 mm	6.6	-----	Cobbles
2.00 mm	22.5	2.2	Pebbles
1.00 mm	14.6	26.1	Sand
500 μm	16.5	29.9	Sand
250 μm	18.3	13.5	Sand
125 μm	13.1	11.0	Sand
53 μm	6.4	5.1	Silt/Clay
< 53 μm	2.0	12.2	Silt/Clay

Reproduced with permission of the copyright owner. Further reproduction prohibited without permission.

yielded a higher silt/clay composition. The particle distribution (Table 4.1) for the dry fiber crete (conducted on July 7, 2000) shows a higher percentage for the smaller grain sizes than the native material (17.6%). Sands still comprise the major portion (80%) with a very small portion being gravels (2.3%).

Table 2.1 lists the moisture content of the native material at 8.8%. This agrees with the observed moisture content during the initial preparation (January 7, 2000) of native material samples for gamma spectroscopy. Sample weights, pre and post drying, showed a moisture content of 8.7% and 8.9%. The moisture content for dry fiber crete (prior to adding water to produce a cured product), measured 1.27% (January 7, 2000). Two other samples measured moisture contents less than 1%. The percent moisture content for cured fiber crete measured approximately 21% (January 14, 2000). This sample was obtained from the .05 drift ribs that was cured for at least one month. The actual drying process occurred two weeks later.

Roelofs and Scholten (1994) noted similar phenomena in that high moisture in concrete, up to 12 months after curing influenced the concrete's exhalation rate. Confirmation of a high moisture content in the cured fiber crete can be observed from Table 3.21, where the six samples used for gamma spectroscopy had approximately 150 ml (each) of industrial water, yielding an estimated 15% water content.

While the cured fiber crete had the highest moisture content of the three material types used in this study, it also had a higher percentage of silts and clays than the native material. Thus the radon within the individual grains were able to emanate more freely than the other two materials.

Reproduced with permission of the copyright owner. Further reproduction prohibited without permission.

A comparison of native material and dry fiber crete emanation coefficients (showing dry fiber crete with the higher coefficient), suggests that grain size and density can play a greater influence than moisture for radon to transfer from the grain and into the pore space. Luetzelschwab et al (1989) observed that prior to saturation of a soil, the moisture content produces a consistent emanation. The emanation changes when the soils become saturated. This suggests that prior to saturation, moisture can influence radon emanation; however, density and grain size may predominate this influence, depending on the degree of saturation and degree of density and grain size.

A comparison of the emanation coefficients to literature values shows the observed emanation coefficient for native materials is low by a factor of 100. Table 1.1 shows the emanation for typical soils to be approximately 0.2. Luetzelschwab et al (1989), measured five different soils and, while measuring similar radon concentrations to those displayed in Tables 3.11 and 3.13, emanation coefficients ranged from 0.15 – 0.42. The coefficients for native materials in this study ranged from 0.0047 to 0.0061. The low coefficient is the result of drying the native material (at 100° C for one week) per the gamma spectroscopy procedure. Therefore, a comparison to moist crushed rock or dried sand with a mean diameter of 20 μm (as listed in Table 1.1) would fall short. The emanation coefficient for the native material should have been conducted with its natural 8.8% moisture content. This would have increased the number of atoms to terminate their migration in the water-filled pore spaces.

Comparing the dried native material to a dried soil of smaller diameter would have also been erroneous. This is because larger grains would decrease the likelyhood of

Reproduced with permission of the copyright owner. Further reproduction prohibited without permission.

radon atoms from penetrating the boundary of their host grain and entering the soil pore spaces.

The difference in coefficients may also be due to variations in soil densities. Densities for the native materials ranged from 1.20 – 1.35 g cm^{-3}, with an average density of 1.28 gr cm^{-3}. Luetzelschwab et al (1989) showed soil densities ranging from 0.9 – 1.7 g cm^{-3} for loose/shaked soils and 1.2 – 1.9 g cm^{-3} for tightly packed soils. Using sandstone as a similar type soil found in the U1a Complex, the density for loose/shaken material was 1.34 g cm^{-3} and 1.8 g cm^{-3} for tightly packed material. As soil compaction increases, the soil has a higher bulk density. This results in less interstitial air space which could cause radon atoms to terminate their path-of-recoil in a neighboring grain (Luetzelschwab et al 1989).

4.3 Exhalation Measurements from Charcoal Canisters

The initial sampling for the passive diffusion charcoal canisters show unexpected results. The data presented in Table 3.31 displays no significant difference in the exhalation values for 171 and 252 hour sampling periods between the native material and fiber crete surfaces. The average values for the fiber crete surface was 26.89 and 10.94 pCi l^{-1} for 171 and 252 hour sampling periods, respectively, while the native material sampling periods of 171 and 252 hour resulted in concentrations of 27.87 and 10.43 pCi l^{-1}. These numbers not only show non-significance, based on a 95% confidence level, but also show a higher value for the 171-hour sampling period than for the 252-hour sampling period.

While laboratory results reported radon activity as airborne concentrations (pCi l^{-1}), mathematical manipulations converted these concentrations into exhalation values of

Reproduced with permission of the copyright owner. Further reproduction prohibited without permission.

Bq $cm^{-2} hr^{-1}$. This was accomplished by converting the net activity count into becquerels and dividing by the canister's surface area (81.07 cm^2) and the exposure time. The conversion value for the average exhalation for 84, 171, and 252 hours for both native material and fiber crete surfaces are presented in Table 4.2.

The unexpected results for the in-situ exhalation values appears to be the result of the canister placement. The original design criteria required that the canisters not be completely sealed to the surface material. The purpose being that pressure build-up inside the canisters would be prevented and therefore, would allow for diffusion to occur freely without the development of a decreased pressure gradient between the material surface and the canister. However, what appears to have occurred was the collection of radon gas from the homogenous circulated air within the underground drift rather than the exhalated gases from the rib surfaces. Results support this as the 84-hour sampling period displays a significant difference between fiber crete and native material surfaces, with the greater activity for the native material than the fiber crete. This was an expected result as the gamma spectroscopy results determined a higher radon activity in the native material than the fiber crete. The 171 and 252 hour sampling periods showed no significant difference, suggesting that steady state conditions were achieved and that the canisters were actually sampling the mixed ambient air, rather than the exhalated gases from the surfaces. Table 3.31 is a statistical comparison of the exhalation rates for all three sampling periods and both surfaces. The one-tailed t-test (comparing two samples with unequal variances) indicates that only the 84-hour samples show a significant difference (based on a 95% significance), while there is no significance between the

Reproduced with permission of the copyright owner. Further reproduction prohibited without permission.

Table 4.2: Average Exhalation Values for First Round Sampling (Bq $cm^{-2} hr^{-1}$)

	84 Hours	171 Hours	252 Hours
Native Material	0.000439	0.00422	0.00115
Fiber Crete	0.000354	0.00399	0.00122

Table 4.3: Average Exhalation Values for Second Round Sampling (Bq $cm^{-2} hr^{-1}$)

	167 Hours
Native Material	0.00209
Fiber Crete	0.00099

Reproduced with permission of the copyright owner. Further reproduction prohibited without permission.

exhalation rates for the fiber crete and native material surfaces for the 171 and 252 hour sampling periods.

An examination of the environmental data (Figure 4.3) shows humidity within the area of the collection point was elevated during the days immediately preceding the collection of the 171-hour collection canisters. Typically, during the work days (Monday - Thursday), the humidity is shown to be approximately 28.0%, with peak readings at approximately 42.0% from 1700 - 0000 (midnight), daily. These peaks are representative of routine dust control measures, whereby the miners wet an area, to suppress surface dust from becoming airborne. While the test area was not wetted, elevated humidity within the area was recorded during the evening hours of each work day.

Starting at 1600 on Friday, 21 April, 2000, a sharp rise in humidity can be observed on the graph, stabilizing at approximately 60% and continuing until 0800 Monday morning, 24 April, 2000, where the humidity sharply drops to 21%. It was an hour later (0900, Monday morning) that the 171-hour canisters were collected.

While the humidity varied throughout the collection period, both temperature and pressure remained fairly constant. Temperature values ranged from 71° F to 75° F, with the majority of time being 73° F. The pressure fluctuated between 13.10 and 13.20 pounds per square inch (psi). During the weekend period of elevated humidity, all three parameters, temperature, pressure and humidity, were recorded to be very stable, with little fluctuation. The pressure was recorded at 13.20 psi, temperature was 74° F, and the humidity was 60%. While elevated humidity was noted during this time period, the following weekend, from Friday evening to Monday morning (28 April - 1 May, 2000), temperature, pressure and humidity were stabilized at 78° F, 13.20 psi and 15 %,

Reproduced with permission of the copyright owner. Further reproduction prohibited without permission.

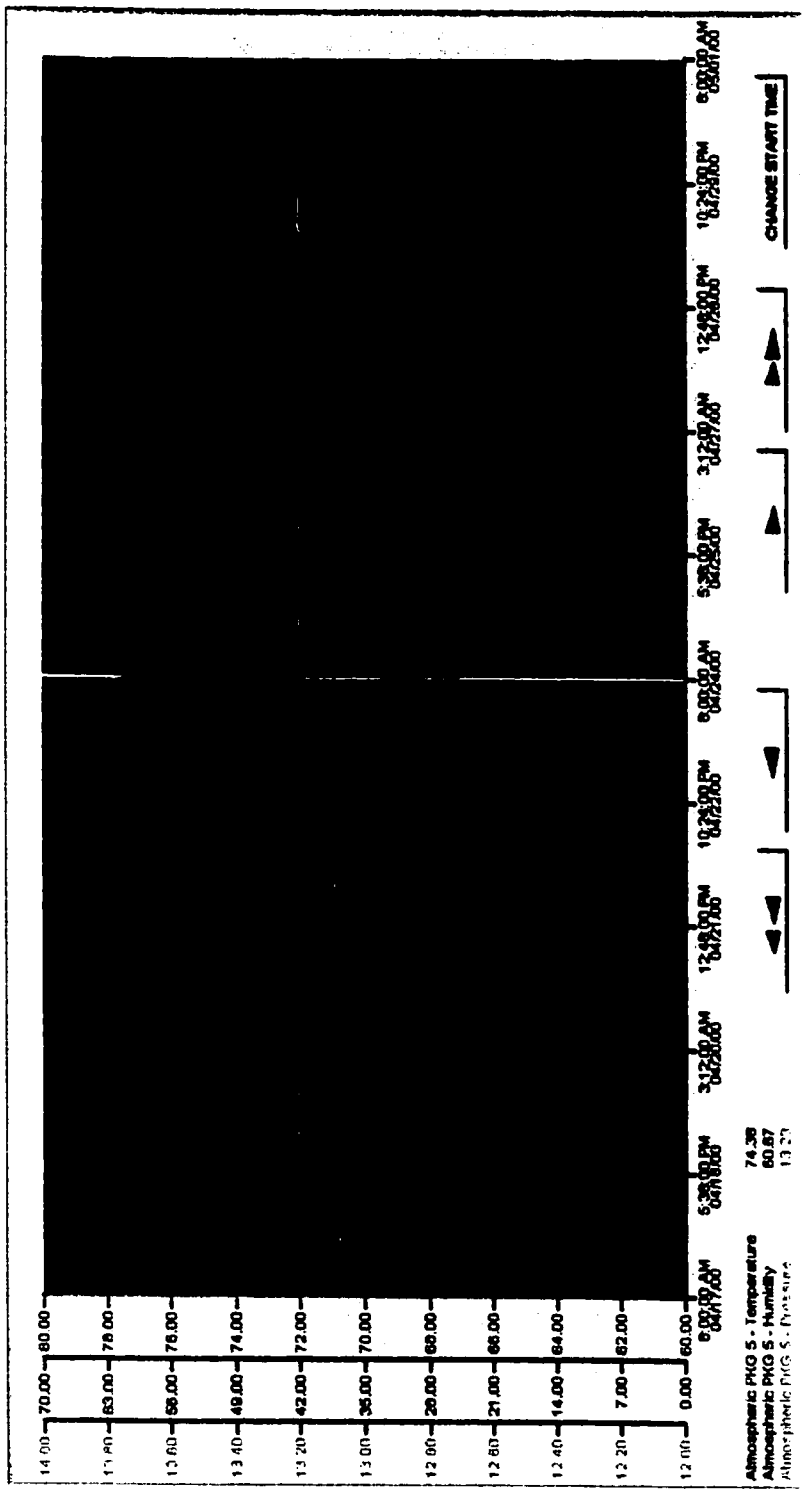

Figure 4.3 Environmental Conditions During First Round Sampling

Reproduced with permission of the copyright owner. Further reproduction prohibited without permission.

Respectively (as the ventilation system remained on). It is interesting to note the difference in humidity between these two weekend periods, showing a variation from 60% to 15%.

Daily reports also indicate that the U1a ventilation system was shut down during the weekend of sampling. As a result, airborne moisture was not removed. Such moist conditions, as presented in the section "Emanation Coefficients" earlier in this report, are optimal for increased radon concentrations due to radon's hydroscopic nature. Therefore, radon's driving force from within the surface material to the wet airborne environment would naturally increase, causing an increased amount of radon into the environment. When the U1a ventilation system was turned back on Monday morning, the humidity quickly returned to the initial conditions (21%). The 252-hour samples were picked up 3½ days later while under the influence of the lower humidity conditions.

While there is no statistical significance between the two 252-hour exhalation rates for the fiber crete and native material surfaces, a large drop in activity occurred from 171 hours to 252 hours. This is an indication of an actual loss of activity. Cohen and Cohen (1983) identify that the adsorption capacity for a passive diffusion charcoal canister is a function of the adsorption charcoal depth. Once saturation is achieved, radon gas can no longer be adsorbed. Saturation is a function of humidity, such that, as moisture enters the charcoal bed, the ability to adsorb is reduced.

Equation 4.1 estimates the time it takes for equilibrium within a charcoal canister to occur. This time is referred to as equilibrium time, t_{eq}, which is the time when the amount of radon gas being absorbed into a passive diffusion charcoal canister, is equal to

Reproduced with permission of the copyright owner. Further reproduction prohibited without permission.

the amount of radon gas, already absorbed in the bed and starts to diffuse out of the canister. This time (which ignores radioactive decay) is expressed as:

$$t_{eq} = h^2 D^{-1} \qquad (4.1)$$

where: h = the depth of the charcoal bed

D = Fick's diffusion coefficient

The determination of D, then becomes a key factor. Such information is typically obtained through experimental data, by varying the exposure times of charcoal canisters, that contain the same amount of charcoal, and conducting gamma spectroscopy to determine the activity per unit surface area at varying depths. Once t_{eq} has been determined, it is of little value to expose that charcoal canister(s) for a time period much larger than this (Cohen, 1983).

While of radon reaches an upper collection limit (due to the charcoal bed's diffusion equilibrium), the decay of radon progeny, ^{214}Pb and ^{214}Bi, progresses (evolvings to its progeny, such as ^{210}Pb) such that any radon collected starts to decay beyond these radionuclides. Therefore, the energy peaks used to identify ^{214}Pb and ^{214}Bi are gradually reduced as these radionuclides decay. Between an adsorption limit for collecting exhalating radon gas (due to a set charcoal bed depth) and the decay of radon's progeny, the ability to collect radon with passive diffusion charcoal canisters can be considerably limited.

Table 4.3 presents data from the second-round sampling for passive diffusion exhalation values from the native material surfaces. Results for the five sealed canisters range from 0.00182 - 0.00241 Bq $cm^{-2} hr^{-1}$. The average value is 0.00209 Bq $cm^{-2} hr^{-1}$. This equates to 5.82 mBq $m^{-2} s^{-1}$. This exhalation rate falls within the literature value,

Reproduced with permission of the copyright owner. Further reproduction prohibited without permission.

cited earlier in this report of 2 - 50 mBq $m^{-2} s^{-1}$ for typical crustal rock exhalation values (NCRP 1988).

A statistical analysis of these samples indicate a significant difference, based on a 95% confidence level. This verifies that the radon exhalation rate for the native material surface is significantly greater than that for the fiber crete surface. Table 3.35 shows the one-tail test to be 0.0000454; well within the 95% criteria.

Porosity, moisture content, permeability and diffusivity all have been recognized as influencing radon exhalation rates (Nazaroff and Nero 1988). Figure 4.5 is a comparison of the in-situ exhalation rates for native materials and cured fiber crete surfaces. While emanation is greater for the cured fiber crete, exhalation is greater for the native materials. Contributing factors appear to be the higher porosity (including diffusivity and permeability) of the native material due to greater pore spaces, plus moisture content.

Permeability, the ability of a fluid to flow through a soil is directly related to pore size and moisture. The reason pertains to smaller mean pore sizes being able to be filled by moisture faster than larger pores. Once the pores are filled, air movement is restricted, and thereby prohibiting radon gas from transferring through the soil and into the open air. Therefore, permeability is reduced in the cured fiber crete surfaces due to its greater moisture content and smaller grain size. Nielson, Rogers and Gee (1984) reported an increase in diffusion as a soil's median pore diameter increases, while it decreases as the water content increases. Therefore, it follows that diffusion is therefore related directly to porosity as seen through Fick's law. As pore size and moisture affect porosity, they also affect diffusivity.

Reproduced with permission of the copyright owner. Further reproduction prohibited without permission.

Roelofs and Scholten (1994) showed that as the content of fly ash increased in concrete, there was an increase in ^{226}Ra. This would lead one to assume an increase in exhalation rates would occur due to an increase in radon production within the material. Observations though, have indicated a decrease in exhalation. Although Roelofs and Scholten do not explain the mechanism of the influence of fly ash, they observed an increase of fly ash content as a component material, resulting in reduced exhalation rates (Roelofs and Scholten 1994). The fiber crete used in this study contains fly ash (as specified in section 2.4 and the company Material Safety Data Sheet); however due to propriety protection, the portion of fly ash used is unknown. Fly ash is a powdery combustion product commonly used in concrete and other building materials. Table 1.2 shows that fly ash has a low emanation of when compared to other typical building materials. Because fly ash is a combustion product (although not burned itself) it would not be found as a constituent in the U1a Complex native material. Thus, the presence of fly ash in fiber crete suggests a reduction in the fiber crete exhalation rate.

Snoddy (1995) concluded that a possible correlation exists between the amount of fly ash, or cement-to-fly ash ratio, and the permeability of concrete. Snoddy determined that while fly ash itself is a porous material, its porous characteristics are negated due to the small particle diameters of the concrete's cement powders that seal the porosities. This reduces the permeability and, in turn, reduce the material's exhalation ability.

Malhorta and Cavette (1982) explained the effects of fly ash from a chemical perspective. Calcium silicate hydrates (C-S-H) are formed when cement is mixed with water. The C-S-H created is crystalline and grows into water spaces. The crystal growth results in the hardening of the cement mix. In addition to the formation of C-S-H, a

Reproduced with permission of the copyright owner. Further reproduction prohibited without permission.

secondary product, calcium hydroxide, is formed. The calcium hydroxide reacts with the fiber crete's remaining fly ash to form additional C-S-H crystals. These crystals grow in the remaining vacant areas, and therefore, predominantly occupy the material's pore spaces. This creates a less porous material with a reduced permeability.

Reproduced with permission of the copyright owner. Further reproduction prohibited without permission.

CHAPTER V

CONCLUSION

5.1 Gamma Spectroscopy

Gamma spectroscopy analysis measured radon progeny activity in the native materials to be approximately twice as great as that for the fiber crete. The average activities for the radon progeny ^{214}Pb and ^{214}Bi, were used to calculate ^{222}Rn activity based on the assumption of equilibrium. The ^{226}Ra activity was subsequently calculated in the same manner. The ^{226}Ra activity for the native material was calculated to be 38 ± 0.9 Bq kg^{-1} and was compared to literature values for common soil-types (30 – 70 Bq kg^{-1}).

5.2 Radon Emanation of Materials

While the calculated ^{226}Ra and ^{222}Rn content in the native material produced activities that were similar to typical soils conditions, emanation coefficients, averaging 0.005 were much less than the coefficients for other similar soils at 0.2. The emanation coefficient for fiber crete averaged 0.07 and was comparable to literature values for concretes at 0.02 – 0.05.

While the low emanation coefficients for native materials is explained by the difference in soil compactions and densities, its lower value, when compared to fiber crete, is the result of less moisture and a larger average pore size. In addition, its emanation was based on its state, rather than its natural moisture content of 8.8%.

Reproduced with permission of the copyright owner. Further reproduction prohibited without permission.

5.3 In-Situ Sampling via Passive Diffusion Charcoal Canisters

The exhalation rate for the native material was approximately twice that of the fiber crete, averaging 0.00209 Bq cm^{-2} hr^{-1} for the native material surfaces and 0.00099 Bq cm^{-2} hr^{-1} for the fiber crete surfaces. The difference in exhalation rates is attributed to the higher moisture content and smaller particle size of the fiber crete. These characteristics contribute to a lower diffusivity for the fiber crete surface, thus reducing the soil gas flow through the medium.

Converting the second round sampling results to Bq m^{-2} hr^{-1}, yields exhalation rates of 21 Bq m^{-2} hr^{-1} and 10 Bq m^{-2} hr^{-1} for the native material and fiber crete, respectively. These numbers are similar to the exhalation rates for concrete materials listed in Table 1.3.

The exhalation rates for the second round sampling determined that the native material contributed a greater amount of radon activity to the underground environment than the fiber crete surfaces; approximately twice as much. This suggests that while fiber crete surfaces can contribute to airborne radon concentrations, the use of fiber creting underground surfaces reduces the airborne radon concentration. This results in a direct influence on radon emanating from the surrounding native material, thus supporting this paper's hypothesis.

Reproduced with permission of the copyright owner. Further reproduction prohibited without permission.

CHAPTER VI

FUTURE WORK

The intent of the first round in-situ measurements was to quantify the radon exhalation rates at different collection periods, such that a curve could be constructed showing an increase in radon activity with respect to collection time. It was anticipated that this curve would have a positive slope that would reach a maximum value which would be maintained at that value based on steady state exhalation conditions. This condition would be considered the actual exhalation rate for a particular material, while the slope would represent specific characteristics for that material (i.e the change in exhalation rate over time, plus the time to reach steady state). Continued studies in this area could result in a characterization of different construction materials based radon exhalation rates.

Another possible area of further study is how radon exhalation rates are influenced by a material's moisture content. This might involve quantifying the change in exhalation rates with respect to time, as the moisture within particular materials gradually decrease. While past studies indicate a certain amount of moisture content increases the radon exhalation rate, saturated materials have a reduced permeability, which results in a reduced exhalation factor. This suggests that each material type has a specific moisture content that yields an optimum exhalation value.

Reproduced with permission of the copyright owner. Further reproduction prohibited without permission.

As certain building materials age, deterioration in the form of cracking may develop. Such deformations may provide a channel for increase diffusion and thus, providing an increased radon exhalation rate. Therefore as fiber crete and other cementaceous age, an increase in radon concentrations could result.

A topic related to the characteristics of the host construction material, is the material's thickness and density. As these material characteristics increase, can the change in exhalation be quantified, such that a one-to-one functional relationship can be observed?

While Roelofs and Scholten showed a relationship between fly ash content and radon exhalation rates, a mechanism needs to be developed which explains this phenomenon, including to what extent fly ash can influence radon exhalation rates (i.e. is there a maximum limit?).

Reproduced with permission of the copyright owner. Further reproduction prohibited without permission.

REFERENCES

Agricola, Georgious. *De Re Metallica*, Translated by Herbert H. Hoover. Originally published, 1556. Dover Publications, Inc. New York City, New York. 1950.

Allen, B.M. "Preliminary Geologic Site Characterization of the LYNER U1A.100 and U1A.101 Drifts, Yucca Flat, Nevada Test Site." Bechtel Nevada. 1996

American Society for Testing and Materials. Designation C 496 – 96. "Standard Test Method for Splitting Tensile Strength of Cylindrical Concrete Specimen." ASTM Phil. Pa. 1996

Bale, W.F., "Hazards Associated with Radon and Thoron; Memorandum to the Files, March 14, 1951." Health Physics. 38: 1062 - 1066. 1980

Bale, W.F., and Shapiro, J.V., "Radiation Dosage to Lungs from Radon and its Daughter Products." In Proc. International Conference on Peaceful Uses of Atomic Energy. Geneva, United Nations, New York. 1956

Barretto, P.M.C., "Emanation Characteristics Terrestrial and Lunar Materials and the Radon-222 Loss Effect on the Uranium-Lead System Discordance." Phd Thesis, Rice University, Houston, Tx. 1973

Budnitz, R.J., , "Radon-222 and its Daughters - A Review of Instrumentation for Occupational and Environmental Monitoring." Health Physics, 26: 145 – 163. Pergamon Press 1974.

Cohen, B.L., Cohen, E.S., "Theory and Practice of Radon Monitoring with Charcoal Adsorption." Health Physics, 45: 501 - 508. Pergamon Press, Ltd. Oxford, England 1983.

Countess, R.J., "^{222}Rn Flux Measurement with a Charcoal Canister." Health Physics, Vol. 31, PP 455-456. Pergamon Press, Ltd. Oxford, England, 1976.

Gray, David J and Windham, Sam T. "NAREL Standard Operating Procedures for Radon-222 Measurement Using Diffusion Barrier Charcoal Canisters." U.S. Environmental Protection Agency, Office of Radiation Programs. Montgomery, Alabama 1990.

Reproduced with permission of the copyright owner. Further reproduction prohibited without permission.

Handbook of Health Physics and Radiological Health 3rd Edition. Shlein, B., Slaback, L.A, Birky, B.K, Williams and Wilkens, Editors. Baltimore, Md. 1998.

International Commission on Radiological Protection, Publication 24. "Radiation Protection in Uranium and Other Mines." Pergamon Press. Oxford, England. 1977.

International Commission on Radiological Protection, Publication 32. "Limits for Inhalation of Radon Daughters by Workers." Pergamon Press. Oxford, England. 1981.

International Commission on Radiological Protection, Publication 50. "Lung Cancer Risk from Indoor Exposures to Radon Daughters." Pergamon Press. Oxford, England. 1987.

International Commission on Radiological Protection, Publication 65. "Protection Against Radon-222 at Home and at Work." Pergamon Press. Oxford, England. 1994.

Kathren, Ronald L. "Radioactivity in the Environment: Sources, Distribution, and Surveillance." Harwood Academic Publications. Amsterdam, Holland. 1984.

Kocher, David C. "Radioactive Decay Data Tables: A Handbook of Decay Data for Application to Radiation Dosimetry and Radiological Assessments." Technical Information Center, U.S. Department of Energy. 1981

Lao, Kenneth Q. "Controlling Indoor Radon: Measurement, Mitigation, and Prevention." Van Nostrand Reinhold, New York. 1990.

Luetzelschwab, J.W., Helweick, K.L., Hurst, K.A. "Radon Concentrations in Five Pennsylvania Soils." Health Physics, 56: 181 - 188. 1989.

Malhorta, V.M., Vavette, G.C. "Silica Fume" Concrete Construction 27 (5) 443 – 446. 1982.

McLaughlin, J.P., and Jonassen, N., "The Effect of Pressure Drops on Radon Exhalation from Walls." In T.F. Gesell and W.M. Lowder (eds.), Natural Radiation Environment III, US Department of Energy, CONF-780422, p.1225. 1980.

Musulin, C.S., Franklin, J.C., Thomas, V.W., "Effect of Diurnal Cycle and Fan Shutdowns on Radon Concentration in an Experimental Uranium Mine." United States Department of the Interior, Bureau of Mines Report of Investigations. PGH, PA. 1982.

National Council on Radiation Protection and Measurements. "Exposure of the Population in the United States and Canada from Natural Background Radiation." National Council on Radiation Protection and Measurements Bethesda, Md. NCRP Publication 94. 1987

Reproduced with permission of the copyright owner. Further reproduction prohibited without permission.

National Council on Radiation Protection and Measurements. "Measurment of Radon and Radon Daughters in Air." National Council on Radiation Protection and Measurements Bethesda, Md. NCRP Publication 97. 1988

National Council on Radiation Protection and Measurements. "Radiation Protection in the Mineral Extraction Industry." National Council on Radiation Protection and Measurements Bethesda, Md. NCRP Publication 118. 1993

National Research Council. "Comparaive Dosimetry of Radon in Mines and Homes." National Academy Press. Washington, D.C. 1991.

National Research Council. "Health Effects of Exposure to Radon." BEIR VI. National Academy Press. Washington, D.C. 1999

National Safety Council. "Fundamentals of Industrial Hygiene," 3rd ed. Plog, Barbara, A. Chicago, Ill 1988.

Nazaroff, William W. and Nero, Anthony V. "Radon and its Decay Products in Indoor Air." John Wiley and Sons. New York, New York. 1988.

Nielson, K.K., Rogers, V.C., Gee, G.W., "Diffusion of Radon Through Soils: A Pore Distribution Model." Soil Science Society of America Journal. 48: 482 - 487. 1984

Pensk, J., Stpiczynska, Z.,and Blaton-Albricka, K. Emanating Power of Radon-222 measured in Building Materials. In T.F. Gesell and W.M. Lowder eds, "Natural Radiation Environment III," US Dept. of Energy, rep CONF-780422. 1980.

Quiring (1968), Quiring, R.F., "Climatological Data Nevada Test Site and Nuclear Rocket Development Station," ESSA Research Laboratories Technical Memorandum - ARL 7, UC-53, Meteorology, TIP-4500 (52nd Ed.), Environmental Sciences Services Administration Research Laboratories, U.S. Department of Commerce, Las Vegas, NV, 89114, August 1968.

Roelofs, L.M.M., Scholten, L.C. "The Effect of Aging, Humidity, and Fly Ash Additive on the Radon Exhalation from Concrete." Health Physics, 67: 266 - 271. 1994.

Rogers, V.C., Nielson, K.K., Holt, R.B. "Radon Diffusion Coefficients for Aged Residential Concretes." Health Physics, 68: 832 - 834; 1995.

Sheldrick, B.H.; Wang, C. Particle Size Distribution. In:Carter, M.R., ed. Soil Sampling and Methods of Analysis. Boca Raton, Fl. Lewis Publishers; 1993.

Shimo, Michikuni, Iida, T., and Ikebe, Y., "Intercomparison of Different Instruments that Measure Radon Concentration in Air." In Hopke, P.K. ed. Radon and its Decay Products. American Chemical Society, Washington, D.C.1987.

Reproduced with permission of the copyright owner. Further reproduction prohibited without permission.

Smith, D.K., Rose, T.P., Davisson, M.L., Hudson, G.B., Niemeyer, S., Moeller, A.E., "Volatile and Fluid Trabsport in Deep, Arid Soils, FY97 LDRD Final Report." Lawreance Livermore National Laboratory. 1998

Snoddy, R., "Laboratory Assessments of the Permeability and Diffusion Characterisitics of Florida Concretes: Phase II, Field Samples and Analysis." The United States Environmental Protection Agency, Office of Research and Development. Washington D.C. 1995

Strandon, E., Kolstad, A.K., and Lind, B. "Radon Exhalation: Moisture and Temperature Dependence." Health Physics, 47: 480 - 484. 1984.

Strong, K.P., Levins, D.M. "Effect of Moisture Content on Radon Emanation From Uranium Ore and Tailings." Health Physics, 42: 27 - 32. 1982.

United States Department of Energy "Annual Site Environmental Report, 1990," 1, DOE/NV/10630-20, DOE Nevada Operations Office, September 1991.

United States Nuclear Regulatory Commission. Code of Federal Regulations. Washington, DC: US Government Printing Office; 10 CFR Part 20: 1992.

Yu, K.N., Chan, T.F., Young, E.C.M. "The Variation of Radon Exhalation Rates from Building Surfaces of Different Ages." Health Physics, 68: 716 - 718; 1995.

Reproduced with permission of the copyright owner. Further reproduction prohibited without permission.

VITA

Graduate College
University of Nevada, Las Vegas

Robert A. Brounstein

Home Address:
3720 Warmbreeze Way
Las Vegas, Nevada 89129

Degrees
Bachelor of Arts, Music, 1977
University of California, Santa Barbara

Bachelor of Science, Chemical Engineering, 1986
California Polytechnic University, Pomona

Thesis Title: The Contribution of Construction Materials to the Airborne Radon Concentrations in an Underground Facility

Thesis Examination Committee:
Chairperson, Dr. Mark J. Rudin, Ph.D.
Committee Member, Dr. William H. Johnson, Ph.D.
Committee Member, Dr. Steen J. Madsen, Ph.D.
Graduate Faculty Representative, Dr. Richard D.Tandy, Ph.D.

Reproduced with permission of the copyright owner. Further reproduction prohibited without permission.